Materials Research. 2026; 29: e20250386
DOI: https://doi.org/10.1590/1980-5373-MR-2025-0386

Chitosan/Collagen Scaffolds Containing Folic Acid: B-Cyclodextrin with Potential Application in Neuronal Tissue Engineering

***Simone Elza dos Santos Teodoro*[1]*, *Luciana de Oliveira Andrade*[2], *Jorge Luís de Melo Guadalupe*[2], *Carlos Alberto Tagliati*[1,3], *Brener Cunha Carvalho*[3], *Ruben Sinisterra*[1,4], *Maria Esperanza Cortés*[1,5]**

[1]Universidade Federal de Minas Gerais, Programa de Pós graduação em Inovação Tecnológica, Av. Presidente Antônio Carlos Presidente Antônio Carlos, 6627, 31270901, Belo Horizonte, MG, Brasil.
[2]Universidade Federal de Minas Gerais, Instituto de Ciências Biológicas, Departamento de Morfologia, Belo Horizonte, MG, Brasil.
[3]Universidade Federal de Minas Gerais, Faculdade de Farmácia, Departamento de Análises Clínicas e Toxicológicas, Belo Horizonte, MG, Brasil.
[4]Universidade Federal de Minas Gerais, Instituto de Ciências Exatas, Departamento de Química, Av. Presidente Antônio Carlos, 6627, Belo Horizonte, 31270901, MG, Brasil.
[5]Universidade Federal de Minas Gerais, Faculdade de Odontologia, Departamento de Odontologia Restauradora, Av. Presidente Antônio Carlos, 6627, Belo Horizonte, 31270901, MG, Brasil.

Received: March 26, 2025; Revised: December 03, 2025; Accepted: January 28, 2026

Folic acid is associated with the growth and development of the nervous system, playing a crucial role in the therapy and differentiation of neural stem cells and the hematopoietic system. In this study, we prepared scaffolds from the biopolymers chitosan and collagen and added the micronutrient folic acid (FA), also known as vitamin B9. We synthesized a scaffold with FA in β-cyclodextrin to prolong the time required for its release. This increased the interaction between the polymeric matrix and Neuro 2A cells. Morphological, chemical and thermal characteristics, cell solutions and adhesion were verified. Cytocompatibility testing on Neuro 2A cells showed that none of the FA-containing scaffolds was harmful to the cells. In fact, FA combined with β-cyclodextrin made the cells more viable and helped them adhere to each other, which made them grow faster. For this reason, scaffolds have potential for use in neuronal tissue engineering as provisional supports for the growth, specialization, and differentiation of neuronal cells.

Keywords: *Scaffolds, Collagen, Chitosan, Folic acid, β-cyclodextrin.*

1. Introduction

The regeneration of nerve tissue has been the subject of research by several scientists since injury affects an individual's quality of life. Neural tissue engineering searches for strategies to eliminate fibrosis and inflammation after implanting materials capable of serving as a scaffold for cell growth. For neural development, scaffolds need to provide a biomimetic environment and keep their structural integrity and stability while they are being used or implanted[1,2].

In neural tissue engineering, an ideal scaffold must have the following characteristics:

(a) allow neuronal survival, proliferation, and migration;
(b) favor cellular electrochemical communication;
(c) absence of toxicity;
(d) possess mechanical properties similar to those of the brain; and
(e) the ability to release substances in a controlled manner[3,4].

An ideal scaffold for use in tissue engineering must have characteristics that mimic the physiological environment. We used the biomaterials chitosan and collagen, along with folic acid and -cyclodextrin, to optimize the scaffolds' structure. Collagen and chitosan are natural polymers that have properties extremely similar to those of living tissues. For the design of scaffolds that offer mechanical support for the growth of neurons, natural hydrogels are the most studied materials[5].

Natural biomaterials have unique microstructures, physiological properties, and a great diversity of constituents[6].

The presence of -NH_2 groups in its chemical structure, when protonated, forms a positively charged chain that promotes cell adhesion and proliferation, making chitosan a widely used biomaterial in tissue engineering[7]. Chitosan serves as a vital component in neuronal tissue engineering materials and has several characteristics that make it an ideal choice in the field of nerve regeneration[8].

Collagen has low mechanical strength, making it necessary to establish cross-links in the material using cross-linking reagents such as glutaraldehyde, diisocyanate,

*e-mail: simone.elza.teodoro@gmail.com
Associate Editor: Rodrigo Orefice
Editor-in-Chief: Luiz Antonio Pessan.

and carbodiimide or by producing composites, such as with chitosan. Electrostatic interactions between the amino groups of chitosan and the carboxyl groups of collagen establish the composite between chitosan and collagen, stabilizing the material's structure and producing a matrix with mechanical properties suitable for scaffolding[9].

Type I, IX, and XVIII collagens are involved in the development of the Central Nervous System (CNS), playing important roles in neural circuit formation, axon guidance, neuronal maturation, and synaptogenesis[10-12].

Folic acid is an essential vitamin for the proper functioning of the human body. Biologically active as tetrahydrofolic acid, folic acid, also known as vitamin B9, forms the myelin sheath in nerve fibers and participates in amino acid metabolism and various biochemical processes such as protein synthesis and nucleic acid synthesis[13-15].

Folic acid (FA) is a multifunctional active substance that has been studied as safe when combined with other chemicals[16]. Researchers in the fields of biomedicine, bioengineering, and regenerative therapies have been paying close attention to this vitamin due to its non-immunogenicity, ability to assist in tissue regeneration and repair, and high stability[16,17]. FA is linked to the development and growth of the nervous system; it is very important for the hematopoietic system and the proliferation and differentiation of neural stem cells[18-20].

Cyclodextrins are macrocyclic short-chain oligosaccharides produced from modified starch. There are three types of cyclodextrins, depending on the number of D-glucopyranose units: 6 units (α), 7 units (β), and 8 units (γ). It is highly bioavailable, non-toxic, and easily modified[21,22]. When cyclodextrins are attached to drugs or form inclusion complexes, they can act as multifunctional transporters[23]. In this study, β-cyclodextrin was used due to its structural characteristics and its excellent clathrate-forming capacity.

One of the most important requirements for the construction of scaffolds at the cellular level is that they be biocompatible and safe in order to be a functional biological structure, allowing cell attachment, migration, and proliferation. It must not be immunogenic or fibrogenic at the tissue level for the body to accept it[24]. Neural tissue engineering scaffolds must mimic the extracellular matrix's natural topography[25].

The selection of a suitable crosslinking agent is crucial to obtain scaffolds with improved properties[26,27]. Therefore, we can carry out chemical crosslinking using crosslinking agents of natural or synthetic origin to form covalent bonds. We used 1-ethyl-3-(3-dimethylaminopropyl) carbodiimide (EDC) because it is a man-made cross-linking agent that can make stable connections with biomaterials. The chemical structure of EDC includes a functional group with the formula RN=C=NR, capable of forming covalent bonds between proteins through the formation of "zero length" amide bonds between the carboxylic and amino groups. Carbodiimide compounds are non-toxic and biocompatible[28,29]. The main goal of this preliminary study was to show that it was possible to add folic acid to chitosan and collagen scaffolds in order to find out what effects the polymeric matrix had on Neuro 2A nerve cells. We cross-linked the scaffolds with carbodiimide to assess their physical-chemical characteristics, controlled release profile, cell viability, and adhesion. We hypothesized that encapsulating folic acid in cyclodextrin would be an effective alternative method to improve the scaffold's properties in the interaction with Neuro 2 A cells. This method would act on the survival, fixation, proliferation, differentiation, and migration of the cells by gradually releasing vitamin B9 into the medium. We developed the scaffolds to serve as temporary matrices in tissue engineering, fostering a favorable microenvironment for cell differentiation and growth. Chemical and physical tests were used to describe the new materials, as well as tests to see how well they worked with rat brain fibroblast and neuroblast cell lines (Neuro-2A).

2. Materials and Methods

2.1. Materials

The materials used for the synthesis were: Vetec glacial acetic acid, Sigma Aldrich low molecular weight chitosan powder deacetylation > 75% (50-190KDa), Fagron Type I hydrolyzed collagen, 99.3% absolute ethyl alcohol - Química Moderna, 95% ethyl alcohol Química Moderna, 1-ethyl-3,3-dimethylaminopropylcarbodiimide hydrochloride Sigma-Aldrich, INFINITY folic acid, Vetec acetone, 37% hydrochloric acid PA Fmaia, P. A Nuclear, Neon sodium bicarbonate, Neon P.A sodium chloride, Vetec anhydrous calcium chloride, Vetec P.A dibasic anhydrous potassium phosphate, Synth Tris-(hydroxymethyl aminomethane), Neon P.A/ACS anhydrous sodium sulfate, and Synth magnesium chloride hexahydrate.

The aqueous solutions were prepared with Milli Q water (Millipore, USA), and the simulated body fluid (SBF) was prepared at the time of use.

Neuro-2A cells (neuroblasts with neuronal morphology derived from mouse brains from the Rio de Janeiro Cell Bank (BCRJ)) were used for cell culture tests. The medium used for cell culture, both during maintenance and in experiments, was DMEM (Sigma) supplemented with 10% fetal bovine serum, 100 µg/mL streptomycin, 100 U/mL penicillin, and 2 mM L-glutamine, all from Gibco.

2.2 Preparation of the scaffolds

Preparation of chitosan solution: 2 g of chitosan were added to 98 mL of deionized water and 2 mL of acetic acid (98%). The mixture was kept under magnetic stirring at room temperature for 30 minutes.

Preparation of type I hydrolyzed collagen solution: 2 g of collagen were added to 100 mL of deionized water at room temperature, under magnetic stirring for 10 minutes.

Preparation of scaffolds: the chitosan (2% w/v) and collagen (2% w/v) solutions were mixed in a volumetric ratio of 70/30 (chitosan/collagen). Folic acid masses were added to this mixture under stirring for 30 minutes, in aliquots according to Table 1 below.

In scaffold QCFACD, we incorporated 20 mg of cyclodextrin into a solution containing 10 mg of folic acid in water at room temperature. We mixed the CD and folic acid in a stoichiometric ratio of 2:1, respectively. We accurately weighed the folic acid, dissolved it in ultrapure water, and dissolved the CD in water using a water bath. Then, we slowly added the folic acid solution to the CD.

Table 1. Composition of the scaffolds.

Scaffolds	Identification	Composition		
		Chitosan (mL)	Collagen (mL)	Folic acid (mg)
QCP	Q:C Pure	70	30	-
QCFA10	Q:C FA 10 mg	70	30	10
QCFACD	Q:C FA 10 mg (β- cyclodextrin)	70	30	10
QCFA20	Q:C FA 20 mg	70	30	20

Add the obtained solution to the 70:30 chitosan-collagen mixture. We froze the solutions at -20°C for 48 hours. After this period, they were freeze-dried using a Savant Mdulyo D-Freeze Dryer, Thermo Electron Corp., for drying the scaffolds at -46 ºC and 1.1 mBar for 3 days.

Chemical crosslinking was carried out using the methodology adapted from Kim et al.[30]. After being removed from the freeze dryer, the samples were placed in a desiccator to come to room temperature and cross-linked. For the crosslinking process, 1% (w/v) of the scaffolds were used for every 0.7% (w/v) of the crosslinking solution of 1 ethyl, 3,3 dimethylaminopropyl carbodiimide hydrochloride diluted in a solution of Acetone: Water (8:2) (v/v) for 24 hours at a temperature of 4°C.

After the cross-linking period, we fully submerged the scaffolds in absolute ethanol for 1 hour, then 70% (v/v) ethanol for 1 hour. We then rinsed them with ultrapure water (v/v) for 30 minutes and finally lyophilized them. (Adapted from Madihally and Matthew[31]).

2.3. Physical and chemical characterization

2.3.1. Microstructural analysis by scanning electron microscopy (SEM)

We fixed the freeze-dried scaffolds in a sample holder with double-sided carbon tape and coated them with gold. Using a JEOL It-300 scanning electron microscope, this process magnifies the sample numerous times, enabling visualization of the material's structure and verification of its chemical elements.

2.3.2. Fourier transform infrared (FT-IR) absorption spectroscopy

The scaffolding was characterized by means of spectroscopic analysis in the infrared region (Fourier transform infrared spectroscopy, FTIR) using a Perkin Elmer Spectrum GX spectrophotometer. We obtained the spectra from KBr pellets in the 4000 to 400 cm-1 regions, using 30 scans and 1 cm^{-1} resolution to identify the characteristic bonds of the scaffolding compositions. We then generated the data using the OriginPro 7.0 program.

2.3.3. Thermogravimetric Analysis (TGA)

The thermal behavior of the scaffolds was studied using thermogravimetric analysis (TGA). The TGA analysis was carried out using a TA Instrument thermal analyzer (model SDT Q600) in a nitrogen atmosphere at a flow rate of 100 mL/min. To assess the loss of mass, the samples were weighed out at around 3 mg in an alumina crucible. The samples were heated at a rate of 10°C per minute up to 750°C. The data obtained was analyzed using OriginPro 7.0.

2.3.4. Porosity and apparent density

We used absolute ethanol as the solvent to determine the porosity and bulk density of the scaffolding, as it does not solubilize the samples and facilitates easy pore penetration. For the analyses, we added a known mass of scaffold (mi) to a beaker containing a known volume of ethanol (v1) and allowed it to stand until the solvent completely immersed the scaffold. We recorded the volume of ethanol remaining in the beaker (v2). After this time, the scaffold is removed from the ethanol and weighed to record its mass impregnated with the liquid (mf). With the values of mi, mf, v1, and v2, its apparent density can be calculated according to Equation 1[32].

$$\rho = \frac{\mathrm{mi}}{(\mathrm{v1} - \mathrm{v2})} \quad (1)$$

The pore volume (Vp) is given by Equation 2, and the density of ethanol is ρ = 0.789 $g.cm^{-3}$.

$$vp = \frac{(\mathrm{mf} - \mathrm{mi})}{\rho\ \mathrm{ethanol}} \quad (2)$$

Porosity (ε) is calculated using Equation 3, described below:

$$\varepsilon = \frac{vp}{(\mathrm{v1} - \mathrm{v2})} \quad (3)$$

2.3.5. Mass absorbency

Mass absorbability (Am) was determined by hydrostatic weighing. A Mettler Toledo XS 104 balance was used. In the first step, the dry scaffolds were weighed (m1). The scaffolds were then soaked in ethanol under reduced pressure. In the subsequent step, the previously moistened structures were removed from the reference liquid, transferred to filter paper to remove excess moisture, and then weighed (m_3). The mass absorbability values were determined according to the following formula:

$$Am = \frac{m3 - m1}{\mathrm{ml}}.100\% \quad (4)$$

Each sample was tested in triplicate and the mean and standard deviation were determined.

2.3.6. Swelling test

The swelling behavior of the scaffolds was carried out using the Swelling Test based on the methodologies of Malik et al.[33] and Ren et al.[34]. For the test, samples of the freeze-dried scaffolds were weighed in triplicate and placed in a PBS pH 7.4 buffer solution at 37°C under agitation at 60 rpm. The experimental times occurred at 10 min, 1 hour, 3 hours and 24 hours, the scaffolds were removed from the PBS, placed on filter paper for 1 second and then weighed.

The swelling ratio was calculated using the following formula:

$$\text{Swelling ratio}\,(\%) = \frac{(\text{final mass} - \text{initial mass})}{(\text{initial mass})}\ \text{x100} \qquad (5)$$

To measure the pH of the scaffold, the methodology was adapted from Lu et al.[35]. We carried out the pH measurements by immersing a sample of each scaffold in 10 mL of artificial body fluid (ABF) and keeping it at intervals of 37 °C. We conducted the test at the following time intervals: 10, 30, 60, and 120 minutes, as well as every 24 hours for 4 days, using a pH meter (MS TECNOPON, mPA-210, Brazil). Every day, we replaced the FCA after each pH measurement. We conducted the tests in triplicate and expressed the values as the average of the measurements for each sample.

2.3.7. Folic acid release

For the folic acid release test, samples of the scaffolds were weighed in triplicate and placed in a 2 mL solution of PBS buffer pH 7.4 at 37 °C under agitation at 55 rpm. The experimental times were 30 min, 1, 3, 5, 7, up to 115 hours, after which the volume was removed and centrifuged for 30 minutes at 3000 rpm. We removed the supernatant and took absorbance readings at a wavelength of 282 nm. We used a UV-visible spectrophotometer (Thermo Scientific Multiscan Spectrum®) for molecular absorption. We changed the PBS medium after each experiment.

We created a calibration curve with known folic acid concentrations, using the PBS pH 7.4 solution as a blank.

2.3.8. Preparation and sterilization of samples

To study the behavior of scaffolds, in vitro cytotoxicity, growth, adhesion, and cell proliferation tests, the scaffolds were prepared under sterile conditions in a laminar flow. In all tests, the scaffolds were previously exposed to ultraviolet (UV) light radiation (254 nm Light Electronics) for 1 hour, at a distance of 10 cm from the radiation source on both sides. For the preparation of the precursor solutions, ultrapure water from the sterile Milli-Q® System was used to obtain the proposed formulations. The sterile scaffolds were subjected to in vitro tests as prepared.

2.4. Cytotoxicity tests, adhesion cellular morphology, and proliferation

Neuro-2a rat brain neuroblast cell lines were used to test the cell culture medium that was exposed to the scaffold for any possible cytotoxicity. DMEM (Sigma) supplemented with 10% fetal bovine serum, 100 g/mL streptomycin, and 100 U/mL penicillin served as the medium for cell culture, both during maintenance and in the experiments. We added 2 mM L-glutamine specifically for cultures and experiments with Neuro-2A cells. The cultures were maintained in a cell incubator at 37ºC and in an atmosphere with 5% CO_2. We submerged each scaffold sample (100 mg) in 10 mL of sterile supplemented DMEM medium and incubated it at 37 °C under orbital rotation at 25 rpm for 72 hours. Following this period, we separated the medium from the hydrogel in aliquots for use in the experiments. We distributed the cells in 96-well plates, with 1 x 10^4 cells per well. A After the incubation period, the plates were washed twice with sterile PBS solution. The medium was then changed to DMEM low glucose without phenol red, and 10 µl of MTT reagent dissolved in PBS at a concentration of 5 mg/mL was added. The plates were protected from light due to the photosensitivity of MTT. After 4 hours of incubation at 37 ºC, 5% CO_2, to form blue formazan crystals, 50 µl of sodium dodecyl sulfate (SDS) detergent solution was added. The absorbance was read at 570 nm in a spectrophotometer (Epoch, BioTek Instruments), and cell viability was represented as a percentage relative to the control. The graphs were generated using GraphPad Prism 6.0 software. The experiments were performed according to Mosmann[36] and based on the guidelines of ISO 10993-5[37] and ECVAM protocol no. 17[38]. According to ISO 10993-5[37] and related protocols, a sample is considered cytotoxic when it shows a reduction in cell viability greater than 30%. Consequently, to be classified as non-cytotoxic, the sample must result in a reduction in viability equal to or less than 30%.

We calculated cytotoxicity using the following formula:

$$\text{Cytotoxicity}\,(\%) = \frac{(\text{Sample absorbance})}{(\text{control group})}\ \text{x100} \qquad (6)$$

The adhesion and cellular morphology of fibroblasts (mouse embryonic fibroblasts, MEF) C57BL/6, spontaneously immortalized in culture[39] and Neuro 2A cells were also examined. For this purpose, the cells were cultured in DMEM-high glucose growth, supplemented with 10% v/v fetal bovine serum and 1% v/v penicillin/streptomycin.

The scaffolds were sectioned using a scalpel to a thickness of 0.3 to 0.5 mm for 3D culture, subsequently placed in 24-well plates (16 mm diameter), and sterilized under UV radiation for 30 minutes. They were subsequently coated with fibronectin for 2 hours. Subsequently, 1x10^5 cells were seeded onto each scaffold using a low volume of 150 µL to facilitate cell adhesion to the biomaterial rather than the plate bottom. After three hours, the well reached a volume of 500 µL. The culture medium was changed bi-daily. In adhesion assays, cells were seeded onto the scaffolds, and after 24 hours, supernatants were collected and transferred to a new tube. The well was thoroughly rinsed with PBS, which was subsequently added to the tube containing the supernatant to maximize cell recovery. Tubes containing well supernatant and PBS from each individual well were centrifuged at 400 g for 7 minutes, and each pellet was resuspended in 50 µL of fresh culture medium. Cell counts were performed utilizing a Neubauer chamber.

$$\text{Adhesion efficiency} = \frac{(\text{Cells initially seeded} - \text{cells in supernatant})}{(\text{Cells initially seeded})} \qquad (7)$$

Fluorescent staining was utilized to evaluate cell morphology by visualizing the actin cytoskeleton. To achieve this, the scaffolds or coverslips with the cells were washed twice with PBS and subsequently fixed with 4% paraformaldehyde at room temperature for 20 minutes. The samples were washed with PBS, permeabilized using 0.5% Triton-X100 for 15 minutes at room temperature, subsequently washed again with PBS, and incubated with Alexa Fluor 546 Phalloidin (Thermo) at a dilution of 1:400 in PBS for 30 minutes at room temperature. The cells were subsequently washed with

PBS, and the cell nuclei were stained with 4',6'-diamino-2-phenyl-indole (DAPI) at a dilution of 1:1,000 in PBS for 1 minute at room temperature. The samples on the scaffolds were initially positioned on coverslips prior to mounting and visualization using a Zeiss LSM 880 confocal microscope at the Center for Image Acquisition and Processing (CAPI) of ICB-UFMG. Three-dimensional videos were obtained utilizing the z-stack configuration.

The proliferation test was conducted following the methodology adapted from Xiao et al.[40]. This experiment utilized mouse fibroblast cells (L929) and Neuro 2A cells were also examined. The specimens, measuring 10 mm in diameter and 2 mm in height, underwent disinfection using ultraviolet radiation for a duration of 1 hour. Subsequently, each sample was individually positioned in the wells of 24-well culture plates, in quadruplicate. To each sample, 400 µL of DMEM low glucose culture medium, supplemented with 20% fetal bovine serum and antibiotics (0.1 mg/mL streptomycin and 100 U/mL penicillin), was added. The plates underwent incubation at 37°C with 5% CO_2 for a duration of 2 hours. Subsequently, the medium was removed, and 200 µL of fresh medium was added to each well. The plates were then incubated for 24, 48, and 72 hours at 5% CO_2. Following the incubation period, the plates underwent two washes with sterile PBS solution. The medium was then replaced with DMEM low glucose, devoid of phenol red, to which 10 µl of MTT reagent, at a concentration of 5 mg/mL, dissolved in PBS, was added. The plates were shielded from light because of the photosensitivity of MTT.

Following a 4-hour incubation at 37 °C in 5% CO_2 to facilitate the formation of blue formazan crystals, 50 µl of sodium dodecyl sulfate (SDS) detergent solution was introduced. Following 15 minutes of agitation, measurements were obtained using a UV-visible spectrophotometer (Thermo Scientific Multiscan Spectrum®) at a wavelength of 570 nm. The graph of cell proliferation was constructed, using culture time as the abscissa and OD value as the ordinate[40,41].

2.5. Statistical analysis

All assays were conducted with three technical replicates and a minimum of two independent experiments were performed. All quantitative data are expressed as means ± standard deviation. Before conducting statistical comparisons, the normality of the data was assessed using the Shapiro-Wilk normality test and the Levene test for homogeneity of variances. ANOVA was employed to evaluate the differences among groups regarding cell viability, proliferation, and adhesion. The Bonferroni post-test was employed to assess significant differences among pairs of groups in multiple comparisons. Significant differences were determined at $p < 0.05$ using the Jamovi project software (2024). Jamovi (version 2.6).

3. Results and Discussion

3.1. Scaffold morphology

Scanning electron microscopy (SEM) images were acquired to analyze the microstructure of the scaffolds. The freeze-dried samples were fractured and subsequently tested for analysis. Formulations QCFACD and QCFA20 exhibit a more porous structure compared to samples QCP and QCFA10, potentially offering increased surface area for cell growth. The images of scaffolds QCFACD and QCFA20 predominantly exhibited rounded and open pores. Figures 1A and 1B, presents the scanning electron microscopy micrographs of the scaffolds synthesized with a Chitosan/Collagen ratio of 70:30.

The incorporation of folic acid and β cyclodextrin modified the morphological characteristics of the polymer matrix, resulting in enhanced porosity with interconnected pores of varying sizes, as illustrated in Figure 1A. Based on these images, the average pore diameter of the material was measured (mean ± standard deviation): QCP 34.92 ± 12, QCFA10 29.67 ± 23, QCFACD 93.94 ± 6 and QCFA20 36.04 ± 17. Sample QCP exhibited a fibrous structure characterized by the presence of pores. The scaffolds containing folic acid exhibited a notable alteration characterized by the presence of pores of diverse sizes, as observed in scaffold QCFACD and QCFA20, which demonstrated evidence of interconnections among them. Scaffold QCFA10 exhibits a less organized structure in comparison to scaffolds QCFACD and QCFA20.

The present study demonstrated the synthesis and characterization of chitosan-collagen scaffolds with the addition of folic acid and the incorporation of β-cyclodextrin.

Figure 1B presents the scanning electron microscopy micrographs of the scaffolds synthesized with a Chitosan/Collagen ratio of 70:30. A highly porous structure with interconnected pores is essential for the attachment and growth of new tissue in a biomaterial[42]. SEM images serve as valuable instruments for predicting the potential migration of cells into biomaterials. SEM images (Figure 1B) facilitate the assessment of scaffold structure and pore diameter. Scanning electron microscopy (SEM) images were acquired to analyze the microstructure of the scaffolds. The images indicate that sample QCFACD features a porous, open structure with interconnected pores, aligning with findings by Grier et al.[43], potentially offering increased surface area for cell growth. The surface exhibits significant roughness and texture, characterized by observable micropores. This structure is designed to enhance cell adhesion by offering multiple attachment sites, facilitate cell migration into the scaffold, and ensure the unobstructed transport of nutrients and metabolites.

To enhance visualization of potential alterations in the cross-sectional surface area, these four samples were further analyzed at increased magnification (Figures 1A and 1B). An increase in the surface roughness of sample QCFACD is observed. This represents a significant benefit in cell culture on scaffolds, offering a site for the attachment of adherent proteins and cells, as demonstrated in prior research in the field. Rahman et al.[44] indicates that an average pore diameter exceeding 0.05 mm is necessary for cell attachment; thus, the findings for scaffold QCFACD may facilitate cell attachment[45-47]. The morphology of the scaffolds is one of the most important properties for application in tissue engineering. In order to ensure cell adhesion and the diffusion of nutrients between the cells and the extracellular matrix to be formed, these matrices must have a structure with high porosity and interconnected pores. For each type of cell and tissue to be repaired, there must be a critical pore size range for each scaffold, which may have variations in size[48].

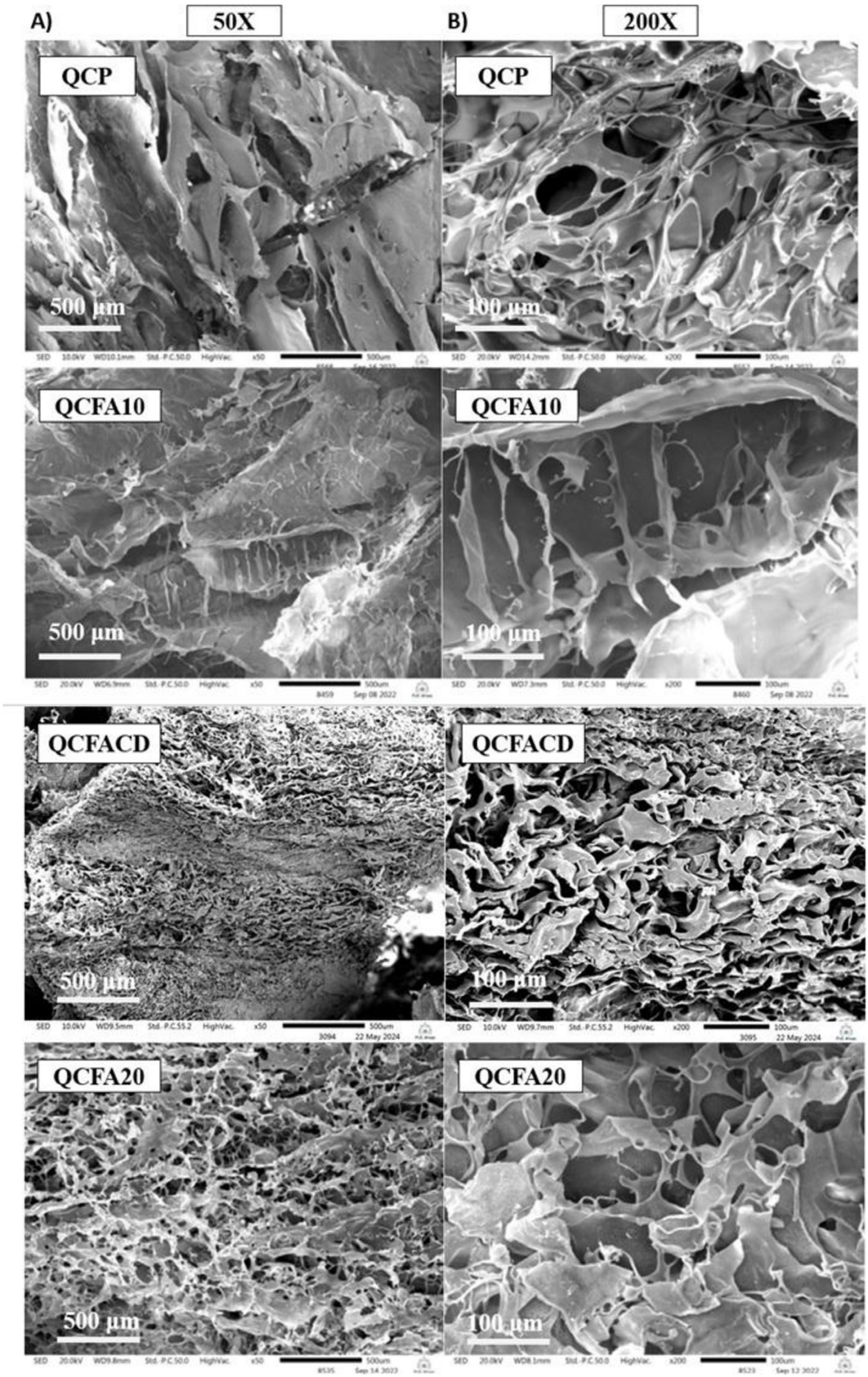

Figure 1. Micrographs of the scaffolds in the scanning electron microscope SEM (A) 50X and B) 200X). QCP; QCFA10, QCFACD and QCFA20 (Q:C Pure, Q:C FA 10 mg, Q:C FA 10 mg β-cyclodextrin and Q:C FA 20 mg) with scale of 500 µm and 100 µm.

For use in tissue regeneration, a suitable material must have a porous structure that allows good circulation of nutrients, cells and removal of metabolic waste[49,50]. The distribution of open and interconnected pores is visible, presenting homogeneous structures with spherical pores. From the images, it is possible to observe that the structure of the matrices changed with the addition of folic acid. The protonated groups of chitosan interact with the deprotonated groups of collagen, leading to intermolecular interactions such as electrostatic and hydrogen bonds formed through the stabilization of collagen fibers[51,52].

The porosity of chitosan-based scaffolds significantly influences properties like cell adhesion, cell proliferation, and swelling capacity, which are critical for tissue growth in tissue engineering[53]. Zhang et al.[47] concluded that smaller diameter pores facilitate cell adhesion. Reduced pore size enhances the retention of physiological fluids and facilitates cell permeation within scaffolds by promoting capillary forces, thereby improving the integration of biomaterials with tissue[54].

3.2. Chemical analysis by FTIR

The analysis conducted through infrared absorption spectroscopy facilitated the characterization of the scaffolds and enabled the identification of bond formation associated with interactions between the chitosan chain, collagen, and the incorporated compounds. The spectrum presented in Figure 2 facilitates the identification of the characteristic absorption bands of the scaffolds.

Figure 2A shows the infrared absorption spectra of the scaffolds and their precursors, hydrolyzed collagen type I, chitosan, folic acid and β cyclodextrin.

Figure 2B shows the FTIR spectra of the raw materials. The typical amide bands of collagen can be observed, such as the amide A band in the region 3720-3120 cm^{-1}, amide B in the region 3115-2815 cm^{-1}, amide I at 1633 cm 4, amide II at 1549 cm^{-1} and amide III at 1243 cm^{-1} [55].

The characteristic absorption band of folic acid can be observed around 3600-2200 cm^{-1} of overlapping vibrations originating from -NH, -OH and -CH bonds; the broadening of the band is due to the presence of numerous hydrogen bonds. Around 1650-800 cm^{-1} we observed overlapping stretching and deformation bands of -C=O, -C-O, -N-H, -C-H bonds of vitamin B9. A characteristic band of folic acid was observed at 768 cm^{-1} attributed to aromatic C-H bending. The band observed at 841 cm^{-1} is a characteristic band of the para-substituted benzene ring[56].

The spectrum of β cyclodextrin was characterized by absorption bands at 3380 cm^{-1} (stretching vibration of -OH), 2925 cm^{-1} (stretching vibration of -C-H) and 1483 cm^{-1} (stretching vibration of the -OH deformation) according to studies by Guo et al.[57].

The objective of this work is to produce scaffolds that function as temporary matrices promoting a diverse distribution of pore sizes facilitating a favorable microenvironment for differentiation and cell growth. Smaller pores facilitate nutrient passage, whereas larger pores provide structural support for cell growth.

Characteristic bands of chitosan were observed at 1073 cm^{-1} and 1033 cm^{-1}, referring to the −CO group in CH_2 −OH and overlapping with the −CO group in the ether-COC- bond (pyranose ring)[58]. The scaffold spectra showed some band shifts in relation to the raw materials (indicated in Figure 2A). The amide I group in the chitosan molecule presents a vibration with a maximum at 1656 cm^{-1} and in the scaffolds with a higher proportion of folic acid, sample QCFA20 with 20 mg of vitamin B9, this peak shifts to 1635 cm^{-1}. The amide II group shifts from 1567 cm^{-1} in chitosan to 1532 cm^{-1} in scaffold QCP; 1558 cm^{-1} in scaffold QCFA10; 1560 cm^{-1} in scaffold QCFACD and 1559 cm^{-1} in scaffold QCFA20. These shifts were also detected by Eslahi et al.[59], and may be indicative of the establishment of hydrogen bonds between the chitosan molecules: collagen with folic acid. The bands shown in the FTIR spectrum of chitosan/collagen scaffolds with added folic acid are consistent with their precursors (Figure 2B) and with the literature[60,61]. It is observed that the spectra present absorption bands characteristic of each component of the formulation. The vibrations of the C=O,

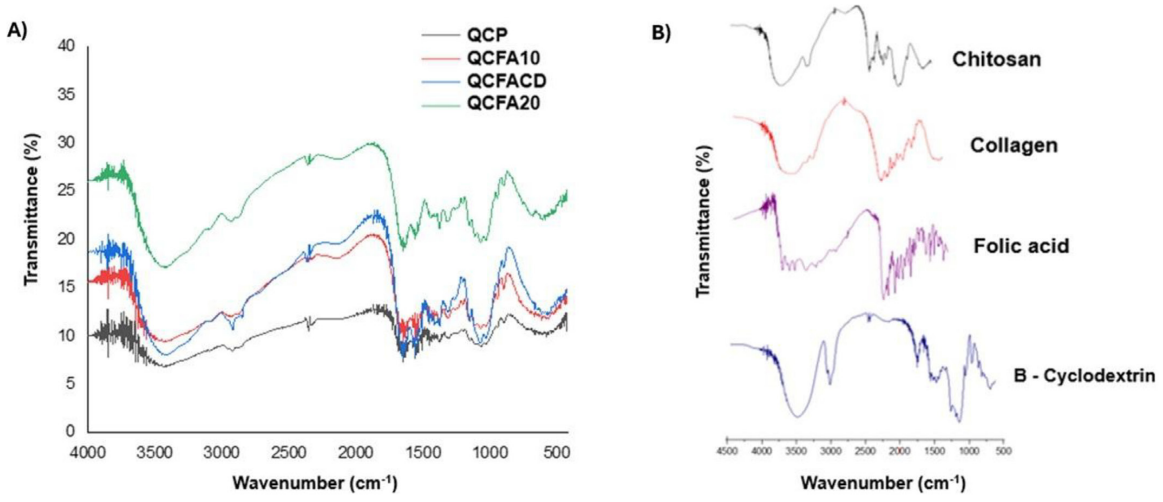

Figure 2. (A) FTIR spectra of the scaffold samples (QCP, QCFA10, QCFACD and QCFA20) Q:C Pure, Q:C FA 10mg, Q:C FA 10mg β-cyclodextrin and Q:C FA 20mg). B) FTIR spectra of the raw materials Chitosan; collagen; Folic acid and β-cyclodextrin.

N-H and C-N bonds characteristic of the amide groups can be observed in the peaks: 1688cm^{-1}, characteristic of C=O stretching (amide I); 1554cm^{-1}, corresponding to NH_2 bending (amide II); 1379 cm^{-1}, mainly referring to C-N stretching. Between 1073-1033cm^{-1} a broad and intense band is associated with cyclic C-O stretching. In the scaffold with 10 mg of folic acid encapsulated with β cyclodextrin (QCFACD), a characteristic peak appeared at 2922 cm^{-1}, which can be attributed to the -C-H stretching vibration[62]. A significant increase was observed in the intensity of the NH vibration band in the scaffolds, corroborating the possibility of establishing intermolecular interactions between the materials[58]. Folic acid is a vitamin capable of binding to different polymers through intermolecular interactions through an interaction of amide II (N-H) with the carboxylic group (C=O), improving stability under different exposure conditions[63]. FTIR analysis also helped to verify such structural changes, whose absorption spectra, in the wavenumber region in which the modifications were observed, an increase in the bands related to the symmetric and asymmetric stretching of the H–C sp^3 bonds, at 2929 cm^{-1} and 2885 cm^{-1}, respectively; change in the absorption bands related to the angular deformation of the $–CH_2$ and $–CH_3$ groups, at 1410 cm^{-1} and 1344 cm^{-1}, respectively; change in the set of bands at 1000-1149 cm^{-1} related to the C–O stretching; Increase in the intensity of the band related to the angular deformation of the –OH group, at 1644 cm^{-1}.

3.3. TGA of the scaffolds

The thermograms of the structures are shown in Figure 3. Thermogravimetric analysis (TGA) was conducted to evaluate the thermal stability and degradation profile of the materials. The QCP structure showed an initial mass loss of 10.49%, with a decomposition temperature of 243.54 °C. The incorporation of folic acid promoted changes in the decomposition temperatures of the scaffolds. The QCFA10 scaffold exhibited a decomposition temperature of 246.36 °C, while the QCFACD formulation, containing β-cyclodextrin, demonstrated greater thermal stability, with decomposition at 260.73 °C. In turn, the QCFA20 scaffold had a decomposition temperature of 244.86 °C.

These results show that the introduction of folic acid and β-cyclodextrin contributes to increasing the thermal stability of the chitosan: collagen matrix. The TG curves obtained in the range of 20 to 750 °C (Figure 3) clearly demonstrate the different stages of mass loss and the effects of structural modifications on the thermal resistance of the materials.

Initially, a mass loss event is observed around 20-120 °C, mainly associated with the elimination of adsorbed water and residual moisture[64]. This behavior is expected for hydrophilic polymeric materials, such as chitosan and collagen, and appears similarly in all samples, although the QCFACD framework shows slightly greater variation in this region, indicating greater water retention or a structure more prone to interaction with solvent molecules.

In the second stage of degradation, located approximately between 200 and 350 °C, more striking differences between the formulations emerge. This interval typically corresponds to the thermal degradation of the main polymer chains, including the rupture of chitosan glycosidic bonds and the thermal denaturation of collagen. It is observed that the curves of the frameworks containing folic acid (QCFA10 and QCFA20) show a subtle shift to higher temperatures compared to the QCP control, suggesting an increase in thermal stability provided by the presence of folic acid. This behavior may be related to the formation of additional intermolecular interactions, such as hydrogen bonds, which tend to delay the onset of thermal decomposition.

The QCFACD scaffold, containing β-cyclodextrin, has the most distinctive profile, with greater thermal resistance and degradation shifted to higher temperatures. The curve shows a smoother thermal transition and a less pronounced loss of mass in the main degradation stage, indicating that β-cyclodextrin plays a significant role in stabilizing the polymer matrix. This improvement may be associated with physicochemical interactions between the functional groups of chitosan/collagen and the hydrophobic cavity of β-cyclodextrin, which may limit the mobility of the polymer chains and reduce susceptibility to thermal breakdown.

At higher temperature ranges (above 450 °C), all samples show a final degradation phase related to the carbonization and oxidation of carbonaceous residues. However, once again, the QCFACD framework retains greater residual mass, demonstrating its greater overall thermal stability. The differences observed reinforce that modifying the matrices with folic acid and, especially, with β-cyclodextrin results in structures with superior thermal properties, which is desirable for applications in biomaterials, especially in situations that require greater resistance to thermal degradation or during processing steps involving heating.

Overall, TG analysis reveals that the additives used play a key role in modifying the thermal behavior of the matrices. β-cyclodextrin showed a more pronounced synergistic effect in stabilizing the system, while folic acid contributed moderately but consistently to delaying degradation. These results demonstrate that the compositional engineering of the chitosan: collagen matrix can be exploited as an effective strategy to optimize its thermal stability and functional performance.

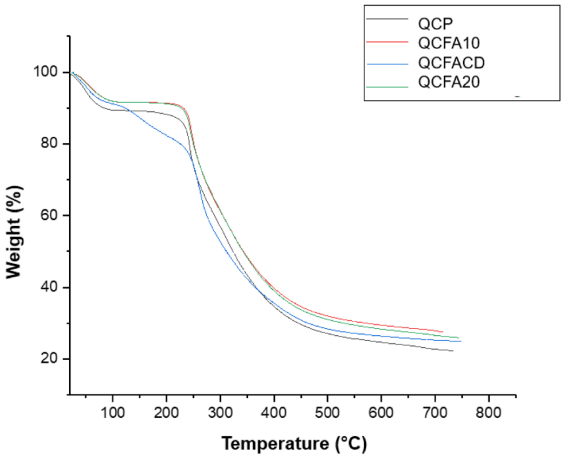

Figure 3. TG curves: analysis of thermal stability (Green) and DTG: mass derivative with respect to time (Blue) of scaffolds QCP, QCFA10, QCFACD and QCFA20.

3.4. Total porosity

The values of scaffold densities and porosity were obtained by calculation using Equations[3-5]. The apparent densities, pore volumes and porosities of the scaffolds are represented in Table 2 with mean ± standard deviation.

The QCFA10, QCFACD, and QCFA20 samples presented higher apparent density and porosity volume values than those observed in the QCP sample, a result that corroborates the evidence previously identified in the morphological analysis by scanning electron microscopy (SEM/MEV). Porosity stands out as one of the most relevant parameters in defining the applicability of scaffolds in tissue engineering, especially because it directly influences cell-material interaction.

Scaffolds with open porosity favor cell filling throughout their volume, allowing adequate nutrient flow and efficient removal of metabolites. Due to this relevance, open porosity was additionally quantified by hydrostatic weighing. It was observed that increasing the concentration of folic acid in the composition of the materials also resulted in an increase in total porosity.

Both porosity and the internal structure of the pores play an essential role in fundamental cellular processes, such as proliferation, differentiation, migration, and tissue regeneration[65]. Structures with larger pores and a higher porous fraction favor gas diffusion, nutrient transport, and the elimination of metabolic waste, promoting greater cellular activity and extracellular matrix (ECM) deposition. On the other hand, smaller pores contribute to a more stable microenvironment, suitable for cell adhesion and adequate intracellular signaling[66,67].

Among the scaffolds analyzed, sample QCFA20—containing 20 mg of folic acid—presented the highest porosity, exceeding the values observed for QCFA10 and QCFACD, a result consistent with the morphological observations obtained by SEM. It is also noteworthy that the QCFACD sample had a higher pore volume compared to the others, a characteristic that can contribute positively to cell behavior.

Structures with well-distributed internal porosity are widely recognized for promoting the adhesion, proliferation, and differentiation of mesenchymal stem cells. According to Li et al.[68], porous scaffolds offer a larger interfacial area for vascularization and bone formation, promoting biological integration between implants and host tissue.

3.5. Mass absorbability

Mass absorbency is an essential parameter in the characterization of polymeric scaffolds intended for tissue engineering, since it determines the material's ability to capture biological fluids and promote its integration with the physiological microenvironment. In the figure presented, it can be observed that the addition of folic acid directly influenced this behavior, as seen in sample QCFA20, which exhibited significantly higher absorbency values compared to the other samples, as indicated in the Figure 4.

Mass absorbability varies similarly to open porosity. The scaffolds modified with folic acid (QCFA10 and QCFA20) presented the highest mass absorbability values, 974% and 1443% respectively. Scaffold QCFACD presented absorbability of 834% compared to scaffold A1, 38% less to the scaffold without the addition of folic acid.

Mass absorbability determines the ability of the scaffold to absorb biological fluids before placement in the patient's body. The results are presented in Figure 4. Scaffold QCP does not have added folic acid, while sample QCFACD has the incorporation of β-cyclodextrin, which may be attributed to the fact that the ethanol solvent was unable to penetrate the entire structure of the scaffold and did not cause high absorbability. Studies carried out on scaffolds for bone regeneration modified with gelatinous coatings of chitosan and folic acid showed higher mass absorbability values for PLA/CS scaffolds after modification with folic acid[69].

3.6. Swelling test

The degree of intumescence of the scaffolds is detailed in Figure 5. This test was performed under isothermal conditions, maintaining the temperature strictly at 37°C to mimic physiological body temperature. The absorption kinetics of the material were investigated by evaluating its behavior at predetermined time intervals.

The Swelling behavior of the dehydrated scaffolds, immersed in PBS, pH 7.4 at 37 ºC, was studied at the experimental times of 10 minutes, 1, 3, and 24 hours.

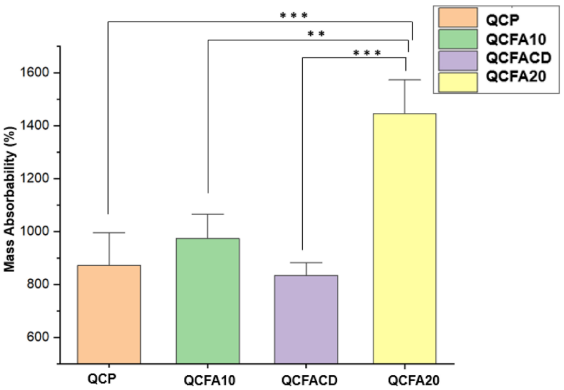

Figure 4. Mass absorbability values of scaffolds QCP, QCFA10, QCFACD and QCFA20 (Q:C Pure, Q:C FA 10 mg, Q:C FA 10 mg β-cyclodextrin and Q:C FA 20 mg). Error bars represent standard deviation values. ANOVA test (* P<0.05, **P<0.01 and ***P<0.001).

Table 2. Apparent densities, pore volumes and porosities of the scaffolds.

Scaffolds	Apparent Density g/cm³	Pore volume cm³	Porosity (ε)
QCP	0.027 ± 0.005	0.058 ± 0.001	0.292 ± 0.003
QCFA10	0.053 ± 0.004	0.065 ± 0.003	0.648 ± 0.032
QCFACD	0.054 ± 0.001	0.108 ± 0.001	0.539 ± 0.001
QCFA20	0.054 ± 0.012	0.100 ± 0.034	1.001 ± 0.338

The data presented are the means of the triplicates Scaffold 1 – (Q:C Pure); Scaffold 2 – (Q:C FA 10mg); Scaffold 3 (Q:C FA 10mg with β CD) and Scaffold 4 (Q:C FA 20mg).

Comparing the scaffolds with each other, at each experimental time, there was a statistically significant difference at 24 hours between the scaffolds: QCP with scaffold QCFACD there was a statistically significant difference $P < 0.001$; QCP with scaffold QCFA20 there was a statistically significant difference $P < 0.01$; QCFA10 with scaffold QCFACD there was a statistically significant difference $P < 0.001$ and QCFACD with scaffold QCFA20 there was a statistically significant difference $P < 0.001$.

At 10 minutes there was a significant difference between scaffold QCP and QCFACD with $P < 0.05$ and between QCFA10 and QCFACD a $P < 0.05$. At 1 and 3h there was no significant difference.

The swelling test (Figure 5) is a technique used to evaluate the diffusion of solvent molecules into the polymer chain, which, when in contact with the material, fills the empty spaces in the chain. Diffusion generates changes in the arrangement of the polymer chain, causing an increase in the volume of the spheres. As the material acquires volume, it causes the spheres to swell, and we can calculate the degree of swelling[70]. All scaffolds are highly swellable, which is related to the presence of hydrophilic groups in the polymer chains. The highest swelling percentage was observed in scaffold QCFACD. In the first 10 minutes of the test, scaffold QCFACD presented a percentage of 2018%. The high initial swelling can be attributed to the flow of water inside the β-cyclodextrin structure, which has a hydrophilic surface and a hydrophobic cavity inside. β-cyclodextrin can form molecular complexes due to possible intermolecular interactions with the environment. The swelling percentage in scaffold QCFACD decreased with increasing immersion time. Scaffolds QCP, QCFA10 and QCFA20 presented higher swelling percentage values in the first 3 hours of analysis. However, a significant decrease in liquid absorption was observed after the experimental time of 24 h. The swelling behaviors of the scaffolds are determined by the interaction with the PBS solution between the hydrophilic and hydrophobic regions, the intermolecular spaces within the polymer network structures, and the pore sizes on the surface. Scaffolds with a large number of hydrophilic functional groups and large pores will swell to a large extent and absorb water many times more than their own weight. While scaffolds with high crosslinking density or with large hydrophobic groups showed a lower swelling percentage[71]. All scaffolds maintained their cylindrical shape and did not dissolve after immersion in PBS. This can be attributed to good crosslinking with 1-ethyl-3-(3-dimethylaminopropyl) carbodiimide. Previous studies have shown that the addition of a crosslinking agent is necessary to improve stability in aqueous media[72].

For biomedical applications, swell behavior is one of the most important parameters. A higher swell percentage results in a larger surface area for the diffusion of bioactives in the environment[73]. Scaffold QCP presented the lowest Swelling ratio at the experimental times of 10 min, 1 h and 3 h. At the time of 24 h, scaffold QCFA10 and QCFA20 presented the lowest Swelling values. Between the times analyzed, scaffold QCFACD presented a decrease in Swelling values, but the highest percentage of the scaffolds studied. The ability to absorb large amounts of aqueous solutions is one of the most significant characteristics of a hydrogel, and can reach hundreds of times its weight[74]. Studies on hydrogels containing chitosan and cellulose presented a high Swelling ratio[75]. The Swelling results found in the experiments of this work correspond to the values found in the literature.

3.7. pH

During the first 10 minutes of incubation of the structures in Artificial Body Fluid (ACF), pH variations were similar among all samples, with the highest values occurring in this initial interval, as illustrated in Figure 6. In all formulations, the results indicated a slightly alkaline pH.

Throughout the four days of incubation, different behaviors were observed. In the QCP, QCFA10, and QCFA20 samples, the pH decreased after the first day, stabilizing between 7.95 and 8.00. In contrast, the QCFACD sample showed an increase in pH values in the first few days, reaching 8.15 on the fourth day (Figure 6B).

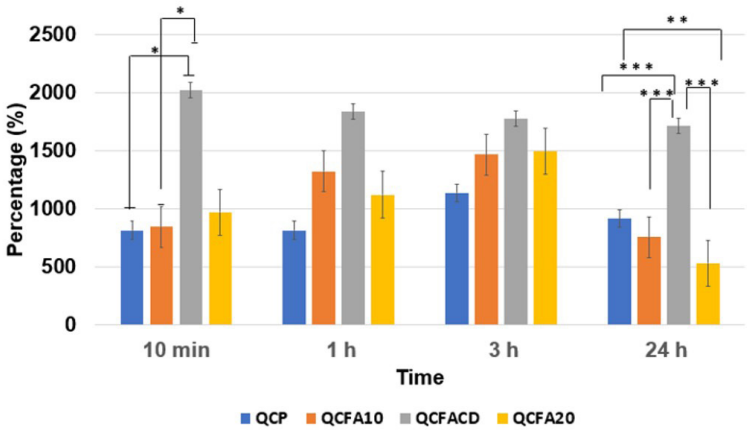

Figure 5. Swelling percentage of scaffolds containing Chitosan and Collagen in the ratio (70:30). QCP, QCFA10, QCFACD and QCFA20 (Q:C Pure, Q:C FA 10 mg, Q:C FA 10 mg β-cyclodextrin and Q:C FA 20 mg). ANOVA test (* $P<0.05$, ** $P<0.01$ and *** $P<0.001$).

These variations suggest the release of ions present in ACF (Na^+, Ca^{2+}, K^+, and Mg^{2+}), which contributes to the increase in pH. This behavior can be considered beneficial, since the initial increase in pH favors both cell adhesion and activity[76].

The analysis of the pH variations of the scaffolds in ACF are shown in Figure 6. Figure 6A shows the pH values in the first 120 minutes. During the preparation of the scaffolds, at the end of the crosslinking, the scaffolds were neutralized. The components of the FCA solution may have interacted when in contact with the scaffolds, altering the pH value to values above 7.00. Determining the pH of the scaffolds is important because changes in these values may occur due to impurities, hydrolysis and decomposition.

To ensure effectiveness in tissue engineering, the biomaterials used in the construction of scaffolds, known as scaffolds, three-dimensional structures of synthetic or natural macromolecules to achieve the expected objective must meet some essential criteria such as biocompatibility, biodegradability, porosity, adhesion, stability, interconnectivity, and allow cell proliferation[77-79].

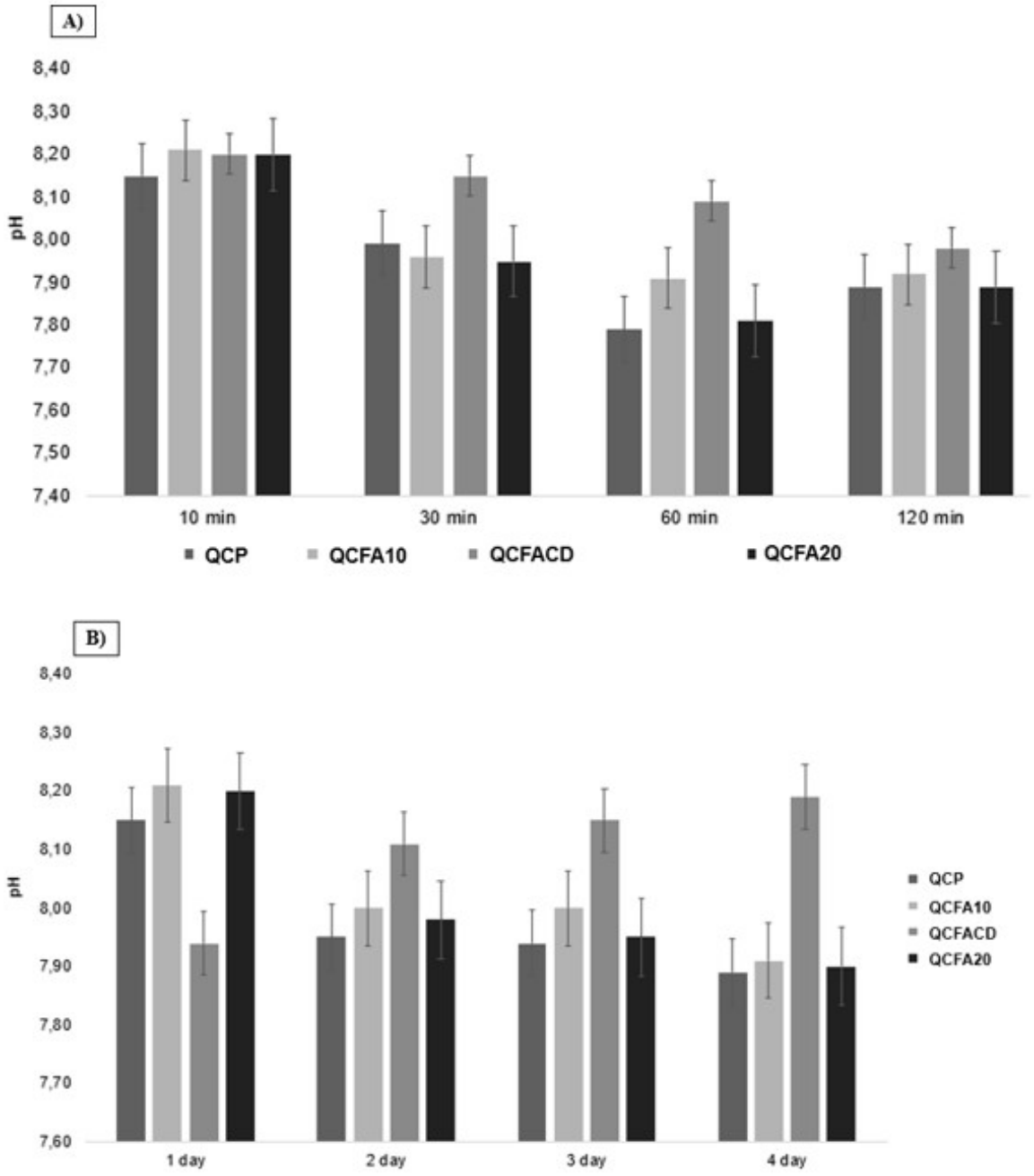

Figure 6. (A) Distribution of pH variation of the scaffold samples of pure Q:C; Q:C FA 10 mg; Q:C FA 10 mg β-cyclodextrin and Q:C FA 20 mg during 120 minutes of sample incubation in simulated body fluid. (B) pH variations after the following 4 days.

Recent studies by Souza et al.[80], demonstrated that U2OS cells showed a 2.25-fold increase in cellular metabolism in single-layer prints prepared at pH 8.0 compared to those prepared at pH 5.5. Cells growing on substrates prepared between pH 7.0 and 8.0 showed an increase in cellular metabolism compared to cells growing on acidic substrates after 7 days of cell culture. Alkaline pH is essential for osteoblast culture, assays performed in acidic medium led to an increase in autophagy and apoptosis of cells[81]. Culture of human fibroblasts and keratinocytes in acidic environments resulted in an increased expression of inflammatory mediators and a reduction in cell migration[82]. On the other hand, it was demonstrated that the pH range between 7.8 and 8.4 increased the growth and differentiation of bone cells, with a slightly alkaline pH being beneficial for MC3T3-E1 cells[83].

3.8. In vitro folic acid release assay

UV-Vis spectroscopy was used to analyze the FA release profile from scaffolds QCFA10, QCFACD and QCFA20. Figure 7 represents the cumulative FA release profiles in samples with PBS buffer solution in vitro at 37°C at pH 7.4 to mimic the pH conditions of systemic circulation.

The evaluation of folic acid release in scaffolds dehydrated in PBS buffer pH 7.4 was performed by immersion in saline solution for a period of 12 days. The data presented are the means of triplicates ($P < 0.001$). Scaffold 2 – (FA 10mg); Scaffold 3 (FA 10mg incorporated in β CD) and Scaffold 4 (FA 20mg).

As shown in Figure 7A, the release curves of scaffolds QCFA10 and QCFA20 showed a rapid release rate in the first 7 h, followed by a slow-release phase. These results

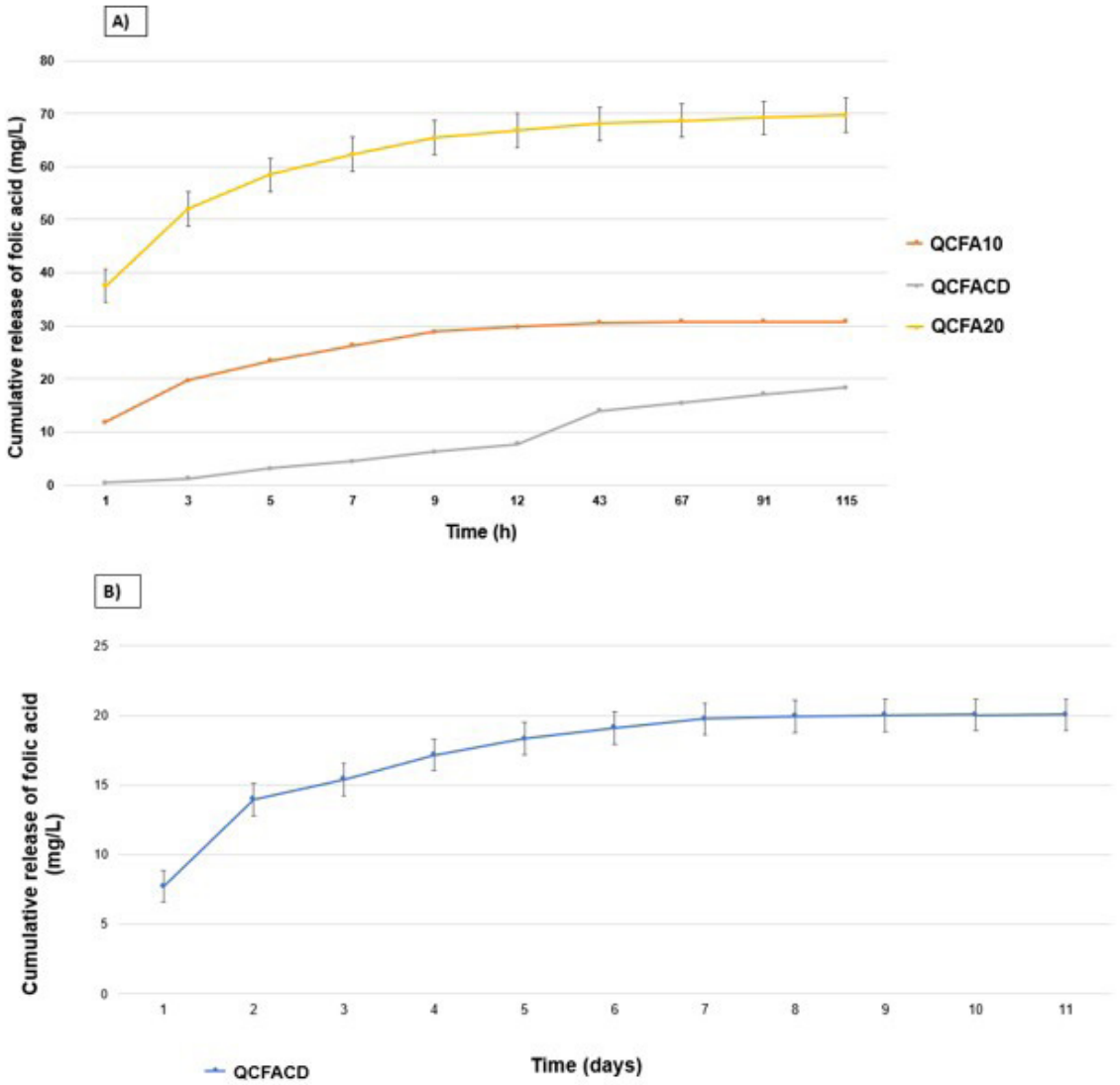

Figure 7. Folic acid release profile in scaffolds QCFA10, QCFACD and QCFA20 in saline solution (PBS, pH 7.4) A) Evaluation of folic acid release in scaffolds QCFA10, QCFACD and QCFA20 in time measured in h; B) Evaluation of folic acid release in scaffold QCFACD in days.

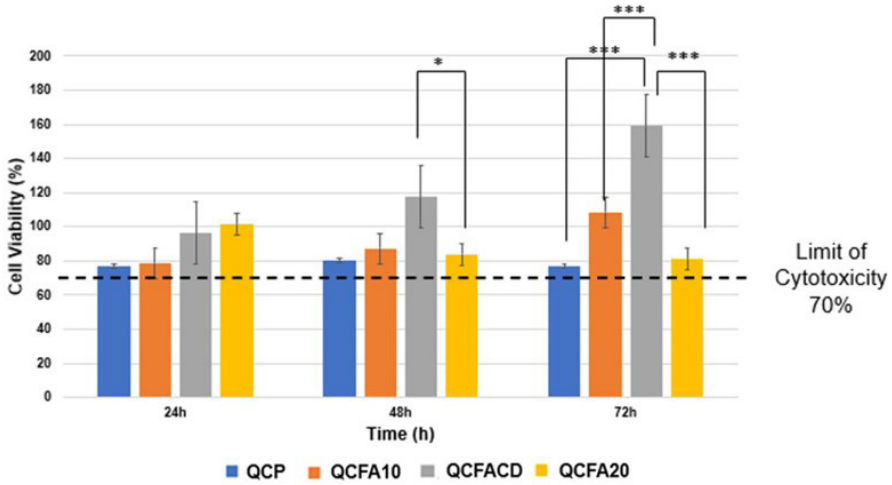

Figure 8. Representation of the L929 indirect contact MTT assay with the scaffold samples of QCP, QCFA10, QCFACD and QCFA20 (Q:C Pure, Q:C FA 10mg, Q:C FA 10mg β-cyclodextrin and Q:C FA 20mg at the experimental time of 24h, 48h and 72 h. ANOVA test (* $P < 0.05$, ** $P < 0.01$ and *** $P < 0.001$).

are consistent with the regulation of vitamin release by free diffusion. Scaffolds QCFA10 and QCFA20 showed rapid release behavior in PBS medium, with a higher dissolution rate than sample QCFACD.

Scaffold QCFACD presented a gradual cumulative release (Figure 7B) profile over the 12 days of testing. This fact may be associated with interactions between β-cyclodextrin and folic acid with the polymer matrix. Thus, it is evident that the incorporation of β-cyclodextrin in the scaffold directly influenced the release kinetics of this vitamin into the medium. These results demonstrate that the folic acid delivery system based on the incorporation of β-CD into the scaffold polymers is extremely useful and important in tissue engineering. The release behavior is estimated to be marked by a high initial value, followed by the release of small doses, or maintenance doses, for a longer time interval, as observed in scaffold QCFACD. The FA release rate in sample QCFA20 during the first day was faster than the other samples. Studies carried out by Alborzi et al.[84], concluded that the drug, or active substance, and the release medium affect the polymer matrix.

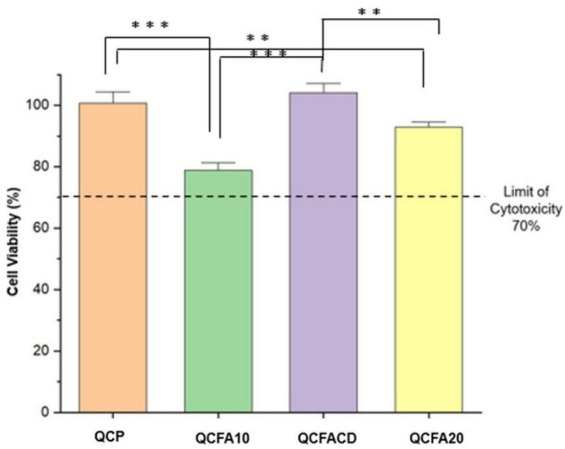

Figure 9. Representation of the Neuro 2A indirect contact MTT assay with the scaffold samples of QCP, QCFA10, QCFACD and QCFA20 (Q:C Pure, Q:C FA 10mg, Q:C FA 10mg β-cyclodextrin and Q:C FA 20mg at the experimental time of 72 h. ANOVA test (* $P < 0.05$, ** $P < 0.01$ and *** $P < 0.001$).

3.9. Cytotoxicity of scaffolds by MTT assay

The results of the MTT tests revealed that after 24, 48 and 72 hours the synthesized scaffolds did not show cytotoxicity to the L929 cell cultures. As shown in Figure 8, the cell viability of scaffold QCFACD (Q:C FA 10mg with β-cyclodextrin) was significantly higher than that of the control group (considered 100%), after 48 and 72 hours. The percentage of viable cells in scaffold QCFACD was 59% higher than in the control group, after 72 hours ($p<0.001$). The viability values remained above 75%, a value above which the materials are considered non-cytotoxic.

The most expressive percentage of cell viability was in scaffold QCFACD followed by scaffold QCFA10. The differences were statistically significant for various study times, as represented in Figure 8.

Figure 8 shows the results of Indirect contact MTT assay of QCP, QCFA10, QCFACD and QCFA20 scaffold samples for 24, 48 and 72 h with L929 fibroblast cells. ANOVA test (* $P<0.05$, ** $P<0.01$ and *** $P<0.001$).

On the other hand, after 48 and 72 hours, the percentage of viable cells in scaffolds QCFACD, QCFA10, and QCFA20 was higher than in sample QCP. Furthermore, after 72 hours, the cell viability of scaffold QCFACD was higher than that of all the scaffolds under study. These initial in vitro results suggest that the addition of folic acid and β-cyclodextrin may have promoted a relatively superior microenvironment, more favorable for the adhesion and development of the cell cultures tested.

Neuro 2A cells (Figure 9) were treated with the media that were in contact with the scaffolds for 72 hours. The viability

in scaffold QCFACD was 104.08%, that is, 4% higher than in the control group. Scaffold QCFACD with 10 mg of folic acid and the incorporation of β-cyclodextrin showed the highest cell viability result, which may be attributed to the controlled release of folic acid into the medium. However, the cell viability of all samples was above 75%, indicating good biocompatibility of all scaffolds. The lower cell viability observed in sample QCFA10 can be justified by the solubility of folic acid in the experimental time of 72 h, which can be attributed to the accelerated leaching of folic acid into the culture medium, which may have acted negatively on the cells and reduced their viability.

Figure 9 Cell viability in Neuro-2A cells for the scaffolds for 72 h.

Statistical analysis was performed between the scaffolds for the cell viability assay. There is a statistical difference between the groups identified by the Tukey Post Hoc ANOVA test between the measurements between: QCP and QCFA10 $p<0.001$; QCP and QCFA20 $p<0.01$; QCFA10 and QCFACD $p<0.001$ and QCFA20 with QCFACD $p<0.01$.

In vitro cytotoxicity analysis was evaluated in terms of cell viability of L929 and Neuro 2A fibroblast cells. In this study, MTT (3-[4,5-dimethyl-thiazol-2-yl]-2,5-diphenyltetrazolium bromide) reduction assays were performed. Scaffold samples QCP, QCFA10, QCFACD and QCFA20 (Q:C Pure, Q:C FA 10 mg, Q:C FA 10 mg β-cyclodextrin and Q:C FA 20 mg) were subjected to in vitro assays. Fibroblast cells were used because these are the main cells involved in wound healing and tissue repair. Fibroblast cells are considered essential for tissue repair due to their great multiplication capacity to fill tissue defects in various organs with an extracellular matrix leading to healing[85].

On the other hand, cytotoxicity was tested in Neuro 2A cell culture to evaluate the possible potential of folic acid and β-cyclodextrin in chitosan: collagen scaffolds in neural cells. Cytotoxicity was performed indirectly using 10 mg/mL dilution of the scaffolds in fibroblast and Neuro 2A cells. The results of cell viability are shown in Figures 8 and 9. L929 fibroblast cells (Figure 8) were treated with the media that were in contact with the scaffolds for 24, 48 and 72 hours. According to the studies by Pal et al.[86], the MTT assay is used to determine cell viability, quantifying how much MTT was reduced by cellular metabolic activity, forming blue formazan crystals. Thus, the amount of formazan, measured by spectrophotometry, is directly proportional to the number of viable cells. As shown in Figure 8, the MTT assay demonstrates the non-toxic nature of the scaffolds produced against the cell types tested.

The determination of cell viability and cell adhesion are extremely important tests, as they measure, in vitro, the first interaction between the cell and the surface of the material, and are a first step in evaluating the potential biocompatibility of the material under study, especially when the material comes into contact with the culture medium and the cells. Folic acid is a vitamin with a hydrophilic character that can help connect Neuro 2A cells to the scaffold surfaces, allowing cell development and improving viability, which is desirable in the context of tissue engineering applications. In the context of tissue engineering applications, it is desirable for the material to have a hydrophilic character to help the cells attach to the surface of the scaffolds, thus facilitating cell growth and increasing their viability[87,88]. All scaffolds are non-toxic and can therefore be used for subsequent exploitation in the manufacture of bioengineered implants/tissues. The results of this study also validate that the polymeric matrix can provide a suitable environment for cell attachment and proliferation, acting as synthetic extracellular matrices.

According to ISO 10993-5[37], for a sample to be considered cytotoxic, there must be a reduction in viability greater than 30% in the cell line evaluated. Therefore, the graphs were marked with a dashed black line at the location where 70% of cell viability is reached. The points on the straight lines of the graphs are representative of the mean ± standard deviation (SD) corresponding to three experimental replicates for each test sample. Studies carried out by Mozafari et al.[89], showed higher cell viability (%) results in composite fibers electrospun with FA compared to the pure ones. This may be attributed to the fact that FA has a high affinity for the folate receptor in L929 cells.

3.10. Adhesion and morphology

Cell adhesion was tested by the cell counting method after the 24-hour incubation period. The result of the adhesion efficiency of L929 and Neuro 2A fibroblast cells adhered to the material after 24 hours is shown in Figures 10 and 11.

After the 24-hour experimental time, the L929 cells exposed to the scaffolds presented adhesion efficiency above 0.9. The scaffold that presented the highest adhesion efficiency, with 0.98, was sample QCFACD with Q:C FA 10 mg and incorporation of β-cyclodextrin (Figure 10).

Figure 11 represents the results of adhesion efficiency in the scaffolds after the 24-hour time with Neuro 2A cells. All scaffolds maintained an adhesion efficiency above 0.8. There was a significant difference between the groups evaluated. Between scaffolds QCP and QCFACD the p-value < 0.05 and between scaffolds QCFACD and QCFA20 the p-value < 0.05.

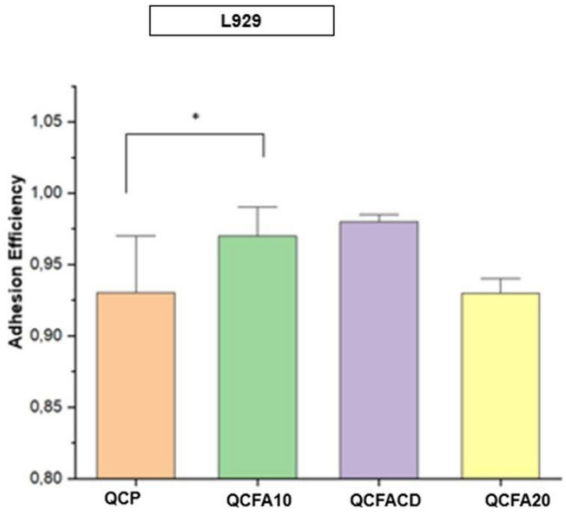

Figure 10. Adhesion efficiency of L929 cells on the scaffolds. ANOVA test (* P < 0.05, ** P < 0.01 and *** P < 0.001).

The morphology and distribution of L929 and Neuro 2A cells are shown in Figures 12 and 13. We can see that L929 cells (Figure 12) were distributed quite uniformly within the scaffold structure after cultivation for 72 hours, as observed on the z axis.

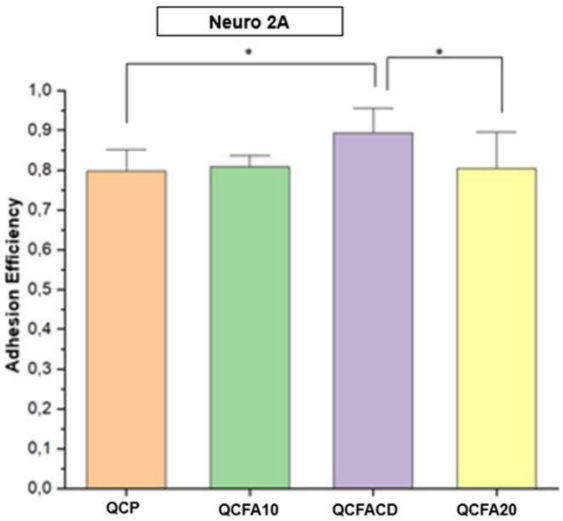

Figure 11. Adhesion efficiency of Neuro 2A cells on the scaffolds. ANOVA test (* $P < 0.05$, ** $P < 0.01$ and *** $P < 0.001$).

We can see in the images shown in Figure 13 that in all scaffolds, Neuro 2A cells adhered to the surface and along the scaffold channels. In both images, Neuro 2A cells proliferated in the scaffolds within 72 hours.

In agreement with the literature, the results of this study demonstrate that the scaffolds exhibited excellent biocompatibility and can promote the proliferation of fibroblasts and Neuro 2A. Furthermore, the cell viability of scaffold QCFACD with folic acid and incorporation of β-cyclodextrin in contact with the cells resulted in higher percentages of cell viability, as can be seen in Figures 8 and 9.

The present in vitro study with neuroblastoma type Neuro 2A and the polymers chitosan: collagen with addition of folic acid and incorporation in β-cyclodextrin, verified favorable evidence for the presentation of this research, which studied the adhesion and proliferation of these cell types on the afore mentioned polymers, through quantitative analysis.

The initial cell adhesion response to the surface of the scaffolds is a very important analysis to assess the biocompatibility of the biomaterials used in the synthesis. The evaluation of cell attachment to the scaffolds was measured in the experimental time of 24 hours. The scaffolds showed a good cell adhesion response, indicating good biocompatibility, as it significantly promoted cell adhesion that could be observed both on the surface of the scaffold and inside the pores.

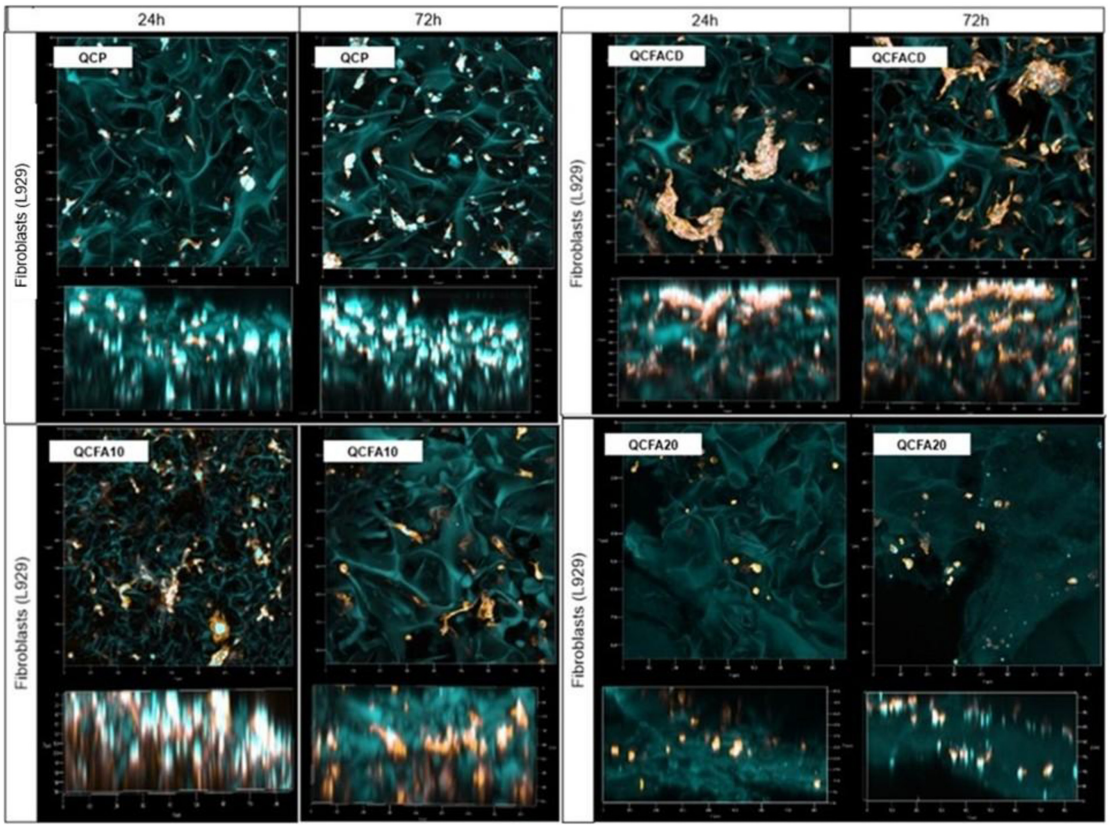

Figure 12. Morphology of L929 cells on the scaffolds at the experimental time 24 hours and 72 hours. ANOVA test (* $P < 0.05$, ** $P < 0.01$ and *** $P < 0.001$).

The encapsulated QC AF 10 mg scaffold (QCFACD) showed a better adhesion efficiency, close to 1.0. The interaction and adhesion of neural cells with artificial substrates are of fundamental importance in neural tissue engineering. The rational design of synthetic neural tissue substrates should achieve maximum control over the assembly and grouping of neural cells. In the central and peripheral nervous systems, neural cells form functional networks where their efficiency depends on the network topology[90-94].

The combination of biomaterials used in the preparation of the scaffolds contributed to a more appropriate environment for cell attachment, favoring their growth and reproduction. These results also suggest that scaffolds based on chitosan and collagen, enriched with folic acid, cross-linked with carbodiimide have great biocompatibility and promote the adhesion and proliferation of Neuro 2A cells. Morphology analysis reveals that cells preferentially align along scaffold grooves (Figure 13), which therefore exert significant influence on cell behavior. The roughness of the scaffold surface, organized at different dimensional scales, appears to cause cells to precipitate into aggregates as observed in sample QCFACD in Figure 13.

Two-photon confocal microscopy was employed to obtain the quantitative localization of individual cells within the scaffold, which may be useful tools for predicting possible cell migration into biomaterials. These results indicate that the scaffold layer not only has good biocompatibility but also significantly promotes cell growth and proliferation.

According to Sung et. al[95], the morphology of Neuro-2A cells on chitosan substrates can be classified into three types[1]: Neuro-2A cells do not present neurite differentiation and are found in rounded form in small clusters in flat regions[2]; Neuro-2A cells with neurite differentiation spreading throughout the biomaterial but not extending to the grooves; and[3], Neuro-2A cells that spread to the grooves with neurite differentiation. In the scaffolds, Neuro-2A cells were spherical in shape, spread across the surface of the scaffolds and in some regions in small clusters. In the cavities, many Neuro-2A cells were observed, identical to those observed by researchers Noguchi et al.[96] and Liu et al.[97]. In the work of Wu et al.[98], glioma cells, regardless of whether they were adhered to each other, presented a spherical morphology when cultured in DMEM medium and 10% fetal bovine serum. The results of the article indicate that Neuro 2A cells evolve to form networks with small-world characteristics by forming small clusters, adhesion and migration being visualized on the z axis, the cells transition from an initial random configuration to a structure with a strong correlation between their internal parts. According to Gentile et al.[99], the small-world network model describes the topology of cell clusters in the scaffolds. Small-world networks elaborate, receive and transmit signals more efficiently than random networks. The main drivers of nerve cell condensation are information maximization and energy minimization. The factors that trigger cell condensation on artificial scaffolds are the nanotopographical features that decorate the surface.

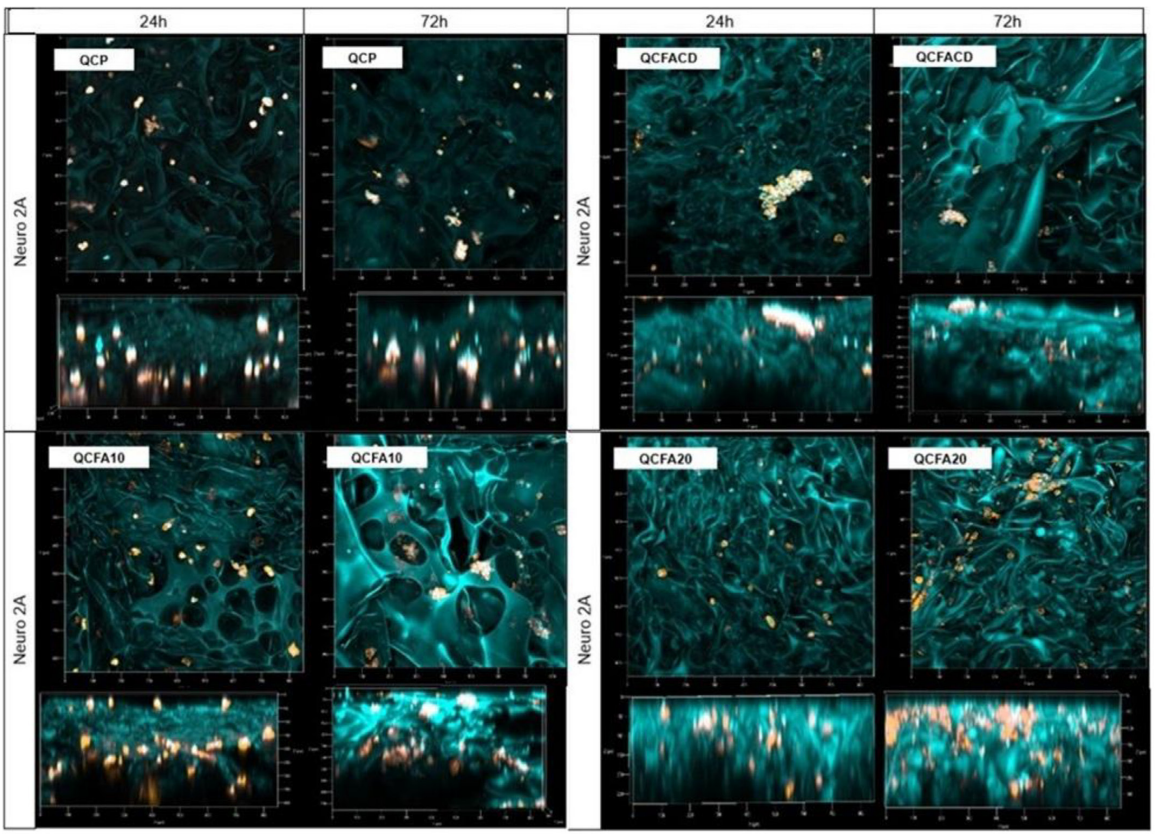

Figure 13. Morphology of Neuro 2A cells in the scaffolds at 24 hours and 72 hours. ANOVA test (* $P < 0.05$, ** $P < 0.01$ and *** $P < 0.001$).

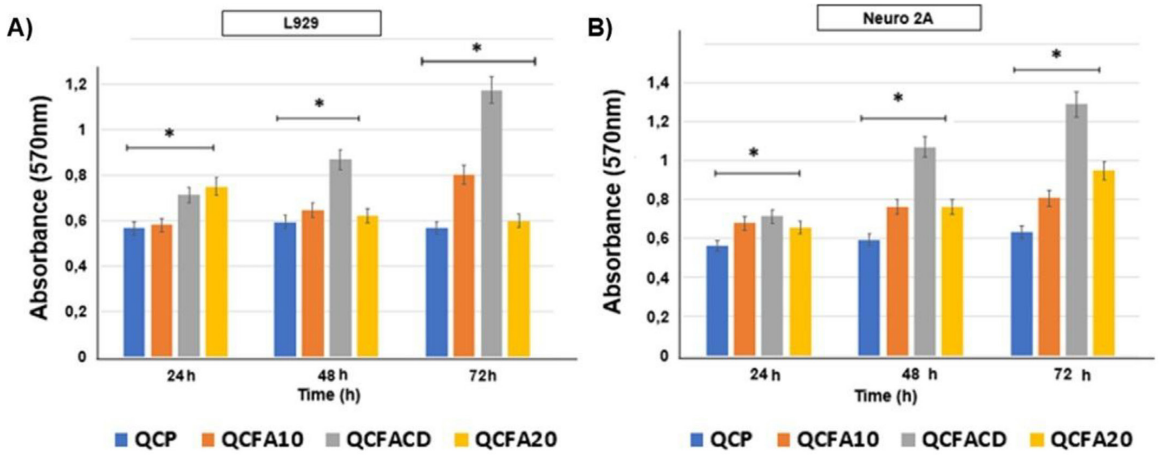

Figure 14. A) Proliferation test of L929 cells seeded on the scaffolds, after 24h, 48h and 72h. **B**) Count of Neuro 2A cells marked by DAPI. ANOVA test (* $P < 0.05$, ** $P < 0.01$ and *** $P < 0.001$).

Understanding the role of surface nanotopography and cellular topology in organizing nerve cells into complex structures may help design strategies for tissue engineering, neuronal regeneration, and nerve repair more quickly and efficiently.

In this study, using images obtained with a Zeiss LSM 880 confocal microscope, the morphology of Neuro 2A cells can be classified as type[1] and demonstrated that the chosen biomaterials have positive characteristics regarding biocompatibility. However, few studies using biomaterials and their application in neuro2A cells have been performed. Therefore, the scarcity of in vitro studies with neuroblastoma type neuro 2A in chitosan and collagen scaffolds with the addition of folic acid, are favorable indications for the presentation of this research, which studied the addition of folic acid to evaluate the adhesion and morphology of these cell types on the scaffolds[95].

3.11. Proliferation test

The proliferation of L929 cells seeded on the scaffold discs was evaluated using the MTT assay (Figure 14). The optical density (O.D.) values provide an indicator of cell growth and proliferation. All developed scaffolds promoted the proliferation of L929 cells after one and three days of experiment. The average O.D. of scaffold QCFACD was higher than that of scaffolds QCP, QCFA10 and QCFA20 in all study periods, but the differences were only significant after 72h. Scaffold QCFACD promoted, after three days, a significantly higher cell proliferation than the other scaffolds.

Figure 14B shows the proliferation test for Neuro 2A cells. The scaffold with the highest proliferation was scaffold QCFACD and QCFA20, which can be attributed to the structure of the material. There was a statistical difference between the groups with $P<0.05$. On the other hand, the QCFACD scaffold containing 10 mg of folic acid promoted significantly greater cell proliferation after three days than the QCP, QCFA10 and QCFA20 scaffolds. The proliferation of L929 cells seeded on the scaffold discs was evaluated using the MTT assay (Figure 14A). The optical density (O.D.) values provide an indicator of cell growth and proliferation. The results indicate that scaffolds QCFA10 and QCFACD acted as a substrate for the growth of fibroblast cells, since the number of cells increased as the culture time extended to 72 h. However, scaffold QCFA20 showed an increase in the 24 h time and a decrease in the 48 h and 72 h times, as can be seen in Figure 14A. Therefore, the scaffolds can be considered cytocompatible, since no obvious negative effects on cell viability were observed. Thus, the excellent proliferative induction results exhibited by scaffold QCFA20 can be explained by the morphology, when compared to the other groups. The results indicate that the scaffolds acted as a substrate for the growth of Neuro 2A cells, since the number of cells in all groups increased as the culture time extended from 24 h to 72 h. Therefore, the scaffolds can be considered cytocompatible, since no negative effects on cell viability were observed. Thus, the excellent cytocompatibility exhibited by the developed scaffolds demonstrates the potential of these biomaterials to favor cell adhesion, spreading and proliferation in Neuro 2A cells.

Thus, this new scaffold has great potential for use in neuronal tissue engineering as a temporary support for the growth, proliferation and migration of Neuro 2A cells.

4. Conclusion

In this study, we prepared hydrogels based on chitosan, collagen, and folic acid as potential scaffolds for tissue engineering. In this study, we made scaffolds carrying folic acid (FA), also known as vitamin B9. We made a compound that included FA in cyclodextrin to extend the time it took to release. The tests that were done and the outcomes about the scaffolds' properties showed that adding folic acid made the system's properties better, mostly in terms of its physicochemical and morphological properties. The images obtained by SEM showed that the addition of vitamin B9 folic acid caused an increase in the pore size in the scaffolds, which may be a relevant factor for the migration of nutrients and cell growth. The study found that scaffolds, specifically QCFACD, with AF: β-cyclodextrin 10 mg, were not cytotoxic and supported the growth of Neuro 2A cells. The scaffolds showed excellent cytocompatibility and showed slow

release in sample QCFACD. The results have advanced our understanding of scaffolds as a matrix for fibroblast and neural cells, promoting cell proliferation and collective adhesion. The biocompatibility of folic acid in scaffolds for temporary growth of healthy cells underscores their significance. These low-cost, easy-to-prepare, and release properties can serve as models for future tissue engineering studies.

5. Acknowledgments

To the Laboratory of Cellular and Molecular Biology of the ICB (Institute of Biological Sciences) of UFMG, to Professor Dr. Paul Saftig (Biochemisches Institut/Christian-Albrechts-Universität Kiel, Germany) for the donation of cells. To the Laboratory of Clinical and Toxicological Analysis of the School of Pharmacy of UFMG. To the Center for Image Acquisition and Processing (CAPI) of ICB-UFMG. To the funding agencies CNPq and Fapemig for their support.

6. References

1. Dehqan Niri A, Karimi Zarchi AA, Ghadiri Harati P, Salimi A, Mujokoro B. Tissue engineering scaffolds in the treatment of brain disorders in geriatric patients. Artif Organs. 2019;43(10): 947-60. https://doi.org/10.1111/aor.13485.
2. Peplow P, Martinez B. Biomaterials and tissue engineering strategies for the treatment of brain neurodegeneration. Neural Regen Res. 2022;17(10):2108. https://doi.org/10.4103/1673-5374.336132.
3. Zhang H, Zhou L, Zhang W. Controlling scaffold degradation in tissue engineering: a review. Tissue Eng Part B Rev. 2014;20(5):492-502. https://doi.org/10.1089/ten.teb.2013.0452.
4. Shafiee A, Atala A. Tissue engineering: toward a new era in medicine. Annu Rev Med. 2017;68(1):29-40. https://doi.org/10.1146/annurev-med-102715-092331.
5. Kaurav H, Kapoor DN. Implantable systems for drug delivery to the brain. Ther Deliv. 2017;8(12):1097-107. https://doi.org/10.4155/tde-2017-0082.
6. Ullah S, Chen X. Fabrication, applications, and challenges of natural biomaterials in tissue engineering. Appl Mater Today. 2020;20:100656. https://doi.org/10.1016/j.apmt.2020.100656.
7. Khan F, Tanaka M. Developing smart biomaterials for tissue engineering. Int J Mol Sci. 2017;19(1):17. https://doi.org/10.3390/ijms19010017.
8. Gu Y, Zhu J, Xue C, Li Z, Ding F, Yang Y, et al. Modified scaffolds with extracellular matrix derived from Schwann cells, based on chitosan/silk fibroin, for filling gaps in the sciatic nerve of rats. Biomaterials. 2014;35(7):2253-63. https://doi.org/10.1016/j.biomaterials.2013.11.087.
9. Parenteau-Bareil R, Gauvin R, Cliche S, Gariépy C, Germain L, Berthod F. Comparative study of bovine, porcine, and avian collagens for the production of a bioengineered dermis. Acta Biomater. 2011;7(10):3757-65. https://doi.org/10.1016/j.actbio.2011.06.020.
10. Sertie AL. Collagen XVIII, which contains an endogenous inhibitor of angiogenesis and tumor growth, plays a critical role in maintaining retinal structure and neural tube closure (Knobloch syndrome). Hum Mol Genet. 2000;9(13):2051-8. https://doi.org/10.1093/hmg/9.13.2051.
11. Fox MA. New roles for collagens in vertebrate nervous system formation. Curr Opin Cell Biol. 2008;20(5):508-13. https://doi.org/10.1016/j.ceb.2008.05.003.
12. Hubert T, Grimal S, Carroll P, Fichard-Carroll A. Collagens in the developing and diseased nervous system. Cell Mol Life Sci. 2009;66(7):1223-38. https://doi.org/10.1007/s00018-008-8561-9.
13. Shulpekova Y, Nechaev V, Kardasheva S, Sedova A, Kurbatova A, Bueverova E, et al. The concept of folic acid in health and disease. Molecules. 2021;26(12):3731. https://doi.org/10.3390/molecules26123731.
14. Li B, Zhang X, Peng X, Zhang S, Wang X, Zhu C. Folic acid and risk of preterm birth: a meta-analysis. Front Neurosci. 2019;13:1284. https://doi.org/10.3389/fnins.2019.01284.
15. Pei P, Cheng X, Yu J, Shen J, Li X, Wu J, et al. Folate deficiency induced histone H2A ubiquitination, leading to downregulation of genes involved in neural tube defects. Epigenetics Chromatin. 2019;12(1):69. https://doi.org/10.1186/s13072-019-0312-7.
16. Fernández-Villa D, Jiménez Gómez-Lavín M, Abradelo C, San Román J, Rojo L. Tissue engineering therapies based on folic acid and other vitamin B derivatives: functional mechanisms and current applications in regenerative medicine. Int J Mol Sci. 2018;19(12):4068. https://doi.org/10.3390/ijms19124068.
17. Taheri A, Jafari SM. Gum-based nanoparticles for the protection and release of bioactive compounds in food. Adv Colloid Interface Sci. 2019;269:277-95. https://doi.org/10.1016/j.cis.2019.04.009.
18. Amarin ZO, Obeidat AZ. Effect of folic acid fortification on the incidence of neural tube defects: folic acid and neural tube defects. Paediatr Perinat Epidemiol. 2010;24(4):349-51. https://doi.org/10.1111/j.1365-3016.2010.01123.x.
19. Liu H, Huang GW, Zhang XM, Ren DL, Wilson J. Folic acid supplementation stimulates Notch signaling and cell proliferation in embryonic neural stem cells. J Clin Biochem Nutr. 2010;47(2):174-80. https://doi.org/10.3164/jcbn.10-47.
20. Stewart KJ, Iskandar BJ, Meier BM, Rizk EB, Hariharan N, Koueik J, et al. Nitrous oxide impairs axon regeneration after nervous system injury in male rats. Anesthesiology. 2019;131(5): 1063-76. https://doi.org/10.1097/ALN.0000000000002906.
21. Periasamy R. A systematic review on the significant roles of cyclodextrins in the construction of supramolecular systems and their potential usage in various fields. J Carbohydr Chem. 2020;39 (5-6):189-216. https://doi.org/10.1080/07328303.2020.1792919.
22. van de Manakker F, Vermonden T, van Nostrum CF, Hennink WE. Cyclodextrin-based polymeric materials: synthesis, properties, and pharmaceutical/biomedical applications. Biomacromolecules. 2009;10(12):3157-75. https://doi.org/10.1021/bm901065f.
23. Shakir M, Jolly R, Khan MS, Rauf A, Kazmi S. Nano-hydroxyapatite/β-CD/chitosan nanocomposite for potential applications in bone tissue engineering. Int J Biol Macromol. 2016;93:276-89. https://doi.org/10.1016/j.ijbiomac.2016.08.046.
24. Levengood SL, Zhang M. Chitosan-based scaffolds for bone tissue engineering. J Mater Chem B. 2014;2(21):3161-84. https://doi.org/10.1039/c4tb00027g.
25. Park S, Kim D, Park S, Kim S, Lee D, Kim W, et al. Nanopatterned scaffolds for neural tissue engineering and regenerative medicine. Adv Exp Med Biol. 2018;1078:421-43. https://doi.org/10.1007/978-981-13-0950-2_22.
26. Thakur VK. Gels horizons: from science to smart materials hydrogels. Singapore: Springer; 2018.
27. Pellá MCG, Lima-Tenório MK, Tenório-Neto ET, Guilherme MR, Muniz EC, Rubira AF. Chitosan-based hydrogels: from preparation to biomedical applications. Carbohydr Polym. 2018;196:233-45. https://doi.org/10.1016/j.carbpol.2018.05.033.
28. Skopinska-Wisniewska J, Tuszynska M, Olewnik-Kruszkowska E. Comparative study of gelatin hydrogels modified by various crosslinking agents. Materials. 2021;14(2):396. https://doi.org/10.3390/ma14020396.
29. Singh P, Nagpal R, Singh UP, Manuja N. Effect of carbodiimide on the structural stability of the resin/dentin interface. J Conserv Dent. 2016;19(6):501-9. https://doi.org/10.4103/0972-0707.194020.
30. Kim HW, Knowles JC, Kim HE. Hydroxyapatite-gelatin composite foams processed by innovative freeze-drying and crosslinking for use as temporary hard tissue scaffolds. J Biomed Mater Res A. 2005;72(2):136-45. https://doi.org/10.1002/jbm.a.30168.
31. Madihally SV, Matthew HW. Porous chitosan scaffolds for tissue engineering. Biomaterials. 1999;20(12):1133-42. https://doi.org/10.1016/S0142-9612(99)00011-3.
32. Loh QL, Choong C. Three-dimensional scaffolds for tissue engineering applications: role of porosity and pore size. Tissue Eng Part B Rev. 2013;19(6):485-502. https://doi.org/10.1089/ten.teb.2012.0437.

33. Malik NS, Ahmad M, Minhas MU, Tulain R, Barkat K, Khalid I, et al. Chitosan/xanthan gum-based hydrogels as potential carriers for an antiviral drug: fabrication, characterization, and safety assessment. Front Chem. 2020;8:50. https://doi.org/10.3389/fchem.2020.00050.
34. Ren B, Chen X, Du S, Ma Y, Chen H, Yuan G, et al. Injectable polysaccharide hydrogel incorporated with hydroxyapatite and calcium carbonate for drug delivery and bone tissue engineering. Int J Biol Macromol. 2018;118:1257-66. https://doi.org/10.1016/j.ijbiomac.2018.06.200.
35. Lu J, Wei J, Yan Y, Li H, Jia J, Wei S, et al. Preparation and preliminary cytocompatibility of magnesium-doped apatite cement with degradability for bone regeneration. J Mater Sci Mater Med. 2011;22(3):607-15. https://doi.org/10.1007/s10856-011-4228-4.
36. Mosmann T. Rapid colorimetric assay for cell growth and survival: application in proliferation and cytotoxicity assays. J Immunol Methods. 1983;65(1-2):55-63. https://doi.org/10.1016/0022-1759(83)90303-4.
37. ISO: International Organization for Standardization. ISO 10993-5: biological evaluation of medical devices – part 5: tests for in vitro cytotoxicity. 3rd ed. Geneva: ISO; 2009.
38. Supino R. DB-ALM protocol nº 17: MTT assay [Internet]. Italy: ECVAM; 1990 [cited 2025 Mar 26]. Available from: http://cidportal.jrc.ec.europa.eu/ftp/jrcopendata/EURL.ECVAM/datasets/DBALM/LATEST/online/DBALM_docs/17_P_MTT%20Assay.pdf
39. Eskelinen EL, Schmidt CK, Neu S, Willenborg M, Fuertes G, Salvador N, et al. Disturbed cholesterol traffic but normal proteolytic function in LAMP-1/LAMP-2 double-deficient fibroblasts. Mol Biol Cell. 2004;15(7):3132-45. https://doi.org/10.1091/mbc.e04-02-0103.
40. Xiao S, Wang M, Wang L, Zhu Y. Environment-friendly synthesis of trace element Zn, Sr, and F codoping hydroxyapatite with non-cytotoxicity and improved osteoblast proliferation and differentiation. Biol Trace Elem Res. 2018;185(1):148-61. https://doi.org/10.1007/s12011-017-1226-5.
41. Lei X, Gao J, Xing F, Zhang Y, Ma Y, Zhang G. Comparative evaluation of the physicochemical properties of nano-hydroxyapatite/collagen and natural bone ceramic/collagen scaffolds and their osteogenesis-promoting effect on MC3T3-E1 cells. Regen Biomater. 2019;6(6):361-71. https://doi.org/10.1093/rb/rbz026.
42. Murphy CM, Haugh MG, Brien Fj O. The effect of average pore size on cell adhesion, proliferation, and migration in collagen-glycosaminoglycan structures for bone tissue engineering. Biomaterials. 2010;31(3):461-6. https://doi.org/10.1016/j.biomaterials.2009.09.063.
43. Grier WK, Tiffany AS, Ramsey MD, Harley BAC. Incorporation of β-cyclodextrin into collagen structures to sequester growth factors and modulate mesenchymal stem cell activity. Acta Biomater. 2018;76:116-25. https://doi.org/10.1016/j.actbio.2018.06.033.
44. Rahman MS, Rana MM, Spitzhorn LS, Akhtar N, Hasan MZ, Choudhury N, et al. Fabrication of biocompatible porous scaffolds based on hydroxyapatite/collagen/chitosan composite for maxillofacial mandibular bone defect restoration. Prog Biomater. 2019;8(3):137-54. https://doi.org/10.1007/s40204-019-0113-x.
45. Kunzler TP, Drobek T, Schuler M, Spencer ND. Systematic study of osteoblast and fibroblast response to roughness by means of surface-morphology gradients. Biomaterials. 2007;28(13):2175-82. https://doi.org/10.1016/j.biomaterials.2007.01.019.
46. Gallyamov MO, Chaschin IS, Khokhlova MA, Grigorev TE, Bakuleva NP, Lyutova IG, et al. Collagen tissue treated with chitosan solutions in carbonic acid for improved biological prosthetic heart valves. Mater Sci Eng C. 2014;37:127-40. https://doi.org/10.1016/j.msec.2014.01.017.
47. Zhang K, Fan Y, Dunne N, Li X. Effect of microporosity on scaffolds for bone tissue engineering. Regen Biomater. 2018;5(2):115-24. https://doi.org/10.1093/rb/rby001.
48. O'Brien FJ. Biomaterials & scaffolds for tissue engineering. Mater Today. 2011;14(3):88-95. https://doi.org/10.1016/S1369-7021(11)70058-X.
49. Camarero-Espinosa S, Rothen-Rutishauser B, Foster EJ, Weder C. Articular cartilage: from formation to tissue engineering. Biomater Sci. 2016;4(5):734-67. https://doi.org/10.1039/C6BM00068A.
50. Tamaddon M, Burrows M, Ferreira SA, Dazzi F, Apperley JF, Bradshaw A, et al. Monomeric, porous type II collagen scaffolds promote chondrogenic differentiation of human bone marrow mesenchymal stem cells in vitro. Sci Rep. 2017;7(1):43519. https://doi.org/10.1038/srep43519.
51. Fernandes LL, Resende CX, Tavares DS, Soares GA, Castro LO, Granjeiro JM. Cytocompatibility of chitosan and collagen-chitosan structures for tissue engineering. Polímeros. 2011;21(1):1-6. https://doi.org/10.1590/S0104-14282011005000008.
52. Sionkowska A, Wisniewski M, Skopinska J, Kennedy CJ, Wess TJ. Molecular interactions in collagen-chitosan mixtures. Biomaterials. 2004;25(5):795-801. https://doi.org/10.1016/S0142-9612(03)00595-7.
53. Ji C, Khademhosseini A, Dehghani F. Enhancement of cell penetration and proliferation in chitosan hydrogels for tissue engineering applications. Biomaterials. 2011;32(36):9719-29. https://doi.org/10.1016/j.biomaterials.2011.09.003.
54. Horn MM, Martins VCA, Guzzi Plepis AM. Interaction of anionic collagen with chitosan: effect on thermal and morphological characteristics. Carbohydr Polym. 2009;77(2):239-43. https://doi.org/10.1016/j.carbpol.2008.12.039.
55. Santos MH, Silva RM, Dumont VC, Neves JS, Mansur HS, Heneine LGD. Extraction and characterization of highly purified collagen from bovine pericardium for potential bioengineering applications. Mater Sci Eng C. 2013;33(2):790-800. https://doi.org/10.1016/j.msec.2012.11.003.
56. Li P, Wang Y, Zeng F, Chen L, Peng Z, Kong LX. Synthesis and characterization of folate-conjugated chitosan and cellular uptake of its nanoparticles in HT-29 cells. Carbohydr Res. 2011;346(6):801-6. https://doi.org/10.1016/j.carres.2011.01.027.
57. Guo J, Zhang L, Wang M, Liu Y, Fei C. Inclusion complexes of etanamizuril with β- and hydroxypropyl-β-cyclodextrin in aqueous solution and in the solid state: a comparative study. Molecules. 2024;29(10):2164. https://doi.org/10.3390/molecules29102164.
58. Kim S, Nimni ME, Yang Z, Han B. Proanthocyanidin-crosslinked chitosan/gelatin films. J Biomed Mater Res B Appl Biomater. 2005;75(2):442-50. https://doi.org/10.1002/jbm.b.30324.
59. Eslahi N, Dadashian F, Hemmati Nejad N, Rabiee M. Evaluation of the incorporation of wool nanoparticles in chitosan/gelatin composite films. J Appl Polym Sci. 2014;131(11):app.40294. https://doi.org/10.1002/app.40294.
60. Milan EP, Rodrigues MÁV, Martins VCA, Plepis AMG, Fuhrmann-Lieker T, Horn MM. Mineralization of phosphorylated fish skin/mangosteen collagen scaffolds as potential materials for bone tissue regeneration. Molecules. 2021;26(10):2899. https://doi.org/10.3390/molecules26102899.
61. Zam ZZ, Muin F, Fataruba A. Identification of chitosan beads from coconut crab patani variety using Fourier Transform Infrared Spectroscopy (FTIR). J Phys Conf Ser. 2021;1832(1):012014. https://doi.org/10.1088/1742-6596/1832/1/012014.
62. Machín R, Isasi JR, Vélaz I. β-Cyclodextrin hydrogels as potential drug delivery systems. Carbohydr Polym. 2012;87(3):2024-30. https://doi.org/10.1016/j.carbpol.2011.10.024.
63. Sudimack J, Lee RJ. Targeted drug delivery via the folate receptor. Adv Drug Deliv Rev. 2000;41(2):147-62. https://doi.org/10.1016/S0169-409X(99)00062-9.
64. Pereira RM, Andrade GSS, Castro HFD, Campos MGN. Performance of Chitosan/Glycerol Phosphate hydrogel as a support for lipase immobilization. Mater Res. 2017;20(Suppl 2):190-201. https://doi.org/10.1590/1980-5373-mr-2017-0091.
65. Gupte MJ, Swanson WB, Hu J, Jin X, Ma H, Zhang Z, et al. Pore size directs bone marrow stromal cell fate and tissue regeneration in nanofibrous macroporous scaffolds by mediating vascularization. Acta Biomater. 2018;82:1-11. https://doi.org/10.1016/j.actbio.2018.10.016.

66. Yao Q, Cosme J, Xu T, Miszuk JM, Picciani P, Fong H, et al. Electrospun three-dimensional nanofibrous PCL/PLA scaffolds with significantly enhanced osteogenic differentiation of stem cells and cranial bone formation. Biomaterials. 2017;115: 115-27. https://doi.org/10.1016/j.biomaterials.2016.11.018.
67. Liu M, Shen Y, Ao P, Dai L, Liu Z, Zhou C. The improvement of hemostatic and wound healing property of chitosan by halloysite nanotubes. RSC Adv. 2014;4(45):23540-53. https://doi.org/10.1039/C4RA02189D.
68. Li Y, Yang C, Zhao H, Qu S, Li X, Li Y. New developments of Ti-based alloys for biomedical applications. Materials. 2014;7(3):1709-800. https://doi.org/10.3390/ma7031709.
69. Bandzerewicz A, Godzieba K, Wierzchowski K, Pilarek M, Gadomska-Gajadhur A. A study of the properties of scaffolds for bone regeneration modified with gel-like coatings of chitosan and folic acid. Gels. 2023;9(10):773. https://doi.org/10.3390/gels9100773.
70. Pasparakis G, Bouropoulos N. Swelling studies and in vitro release of verapamil from calcium alginate and calcium alginate-chitosan beads. Int J Pharm. 2006;323(1-2):34-42. https://doi.org/10.1016/j.ijpharm.2006.05.054.
71. Zhou Q, Yang K, He J, Yang H, Zhang X. A novel 3D-printable hydrogel with high mechanical strength and shape memory properties. J Mater Chem C Mater Opt Electron Devices. 2019;7(47):14913-22. https://doi.org/10.1039/C9TC04945B.
72. Kaczmarek B, Sionkowska A, Osyczka AM. The comparison of physic-chemical properties of chitosan/collagen/hyaluronic acid composites with nano-hydroxyapatite cross-linked by dialdehyde starch and tannic acid. Polym Test. 2017;62:171-6. https://doi.org/10.1016/j.polymertesting.2017.06.027.
73. Holback H, Yeo Y, Park K. Hydrogel swelling behavior and its biomedical applications. In: Rimmer S, editor. Biomedical hydrogels: biochemistry, manufacture, and medical applications. Cambridge: Woodhead Publishing; 2011. p. 3-24. https://doi.org/10.1533/9780857091383.1.3.
74. Elsayed MM. Hydrogel preparation technologies: relevance kinetics, thermodynamics and scaling up aspects. J Polym Environ. 2019;27(4):871-91. https://doi.org/10.1007/s10924-019-01376-4.
75. Barros SC, Silva AA, Costa DB, Cesarino I, Costa CM, Lanceros-Méndez S, et al. Thermo-sensitive chitosan–cellulose derivative hydrogels: swelling behaviour and morphologic studies. Cellulose. 2014;21(6):4531-44. https://doi.org/10.1007/s10570-014-0442-9.
76. Lee GH, Makkar P, Paul K, Lee B. Incorporation of BMP-2 loaded collagen-conjugated BCP granules in calcium phosphate cement-based injectable bone substitutes for improved bone regeneration. Mater Sci Eng C. 2017;77:713-24. https://doi.org/10.1016/j.msec.2017.03.296.
77. Kim CH, Park SJ, Yang DH, Chun HJ. Chitosan for tissue engineering. In: Chun HJ, Park K, Kim CH, Khang G, editors. Novel biomaterials for regenerative medicine. Singapore: Springer; 2018. p. 475-85. https://doi.org/10.1007/978-981-13-0947-2_25.
78. Ahmed S, Annu, Ali A, Sheikh J. A review on chitosan centred scaffolds and their applications in tissue engineering. Int J Biol Macromol. 2018;116:849-62. https://doi.org/10.1016/j.ijbiomac.2018.04.176.
79. Feliciano AJ, van Blitterswijk C, Moroni L, Baker MB. Realizing tissue integration with supramolecular hydrogels. Acta Biomater. 2021;124:1-14. https://doi.org/10.1016/j.actbio.2021.01.034.
80. Souza A, Parnell M, Rodriguez BJ, Reynaud EG. Role of pH and crosslinking ions on cell viability and metabolic activity in alginate-gelatin 3D prints. Gels. 2023;9(11):853. https://doi.org/10.3390/gels9110853.
81. Zhang Z, Lai Q, Li Y, Xu C, Tang X, Ci J, et al. Acidic pH environment induces autophagy in osteoblasts. Sci Rep. 2017;7(1):46161. https://doi.org/10.1038/srep46161.
82. Kruse CR, Singh M, Targosinski S, Sinha I, Sørensen JA, Eriksson E, et al. The effect of pH on cell viability, cell migration, cell proliferation, wound closure and wound reepithelialization: in vitro and in vivo study. Wound Repair Regen. 2017;25(2):260-9. https://doi.org/10.1111/wrr.12526.
83. Galow AM, Rebl A, Koczan D, Bonk SM, Baumann W, Gimsa J. Increased osteoblast viability at alkaline pH in vitro provides a new perspective on bone regeneration. Biochem Biophys Rep. 2017;10:17-25. https://doi.org/10.1016/j.bbrep.2017.02.001.
84. Alborzi S, Lim L-T, Kakuda Y. Release of folic acid from sodium alginate-pectin-poly(ethylene oxide) electrospun fibers under in vitro conditions. Lebensm Wiss Technol. 2014;59(1):383-8. https://doi.org/10.1016/j.lwt.2014.06.008.
85. Harris GM, Madigan NN, Lancaster KZ, Enquist LW, Windebank AJ, Schwartz J, et al. Nerve guidance by a decellularized fibroblast extracellular matrix. Matrix Biol. 2017;60–61:176-89. https://doi.org/10.1016/j.matbio.2016.08.011.
86. Pal K, Banthia AK, Majumdar DK. Polymeric hydrogels: characterization and biomedical applications. Des Monomers Polym. 2009;12(3):197-220. https://doi.org/10.1163/156855509X436030.
87. Nista SVG, Bettini J, Mei LHI. Coaxial nanofibers of chitosan-alginate-PEO polycomplex obtained by electrospinning. Carbohydr Polym. 2015;127:222-8. https://doi.org/10.1016/j.carbpol.2015.03.063.
88. Maretschek S, Greiner A, Kissel T. Electrospun biodegradable nanofiber nonwovens for controlled release of proteins. J Control Release. 2008;127(2):180-7. https://doi.org/10.1016/j.jconrel.2008.01.011.
89. Mozafari M, Moztarzadeh F, Jalali N, Alhosseini SN, Asgari S, Dodel M, et al. Synthesis and characterization of electrospun polyvinyl alcohol nanofibrous scaffolds modified by blending with chitosan for neural tissue engineering. Int J Nanomedicine. 2012;7:25-35. https://doi.org/10.2147/IJN.S25376.
90. Hopfield JJ. Neural networks and physical systems with emergent collective computational abilities. Proc Natl Acad Sci USA. 1982;79(8):2554-8. https://doi.org/10.1073/pnas.79.8.2554.
91. Watts DJ, Strogatz SH. Collective dynamics of "small-world" networks. Nature. 1998;393(6684):440-2. https://doi.org/10.1038/30918.
92. Kandel ER, Schwartz JH, Jessell TM. Principles of neural science. 4th ed. New York: McGraw-Hill; 2000.
93. Watts DJ, Bak P. Small worlds: the dynamics of networks between order and randomness. Phys Today. 2000;53(11):54-5. https://doi.org/10.1063/1.1333299.
94. Strogatz SH. Exploring complex networks. Nature. 2001;410(6825):268-76. https://doi.org/10.1038/35065725.
95. Sung CY, Yang CY, Chen WS, Wang YK, Yeh JA, Cheng CM. Investigating neural cell behavior through micro/nanopatterned chitosan substrates. Biofabrication. 2015;7(4):045007. https://doi.org/10.1088/1758-5090/7/4/045007.
96. Noguchi S, Sumida T, Ogawa H, Tada M, Takahata K. Effects of oxygenated carotenoid β-cryptoxanthin on morphological differentiation and apoptosis in Neuro2a neuroblastoma cells. Biosci Biotechnol Biochem. 2003;67(11):2467-9. https://doi.org/10.1271/bbb.67.2467.
97. Liu H, Kojima N, Kurosawa N, Tsuji S. Regulated expression system for GD3 synthase cDNA and induction of differentiation in Neuro2a cells. Glycobiology. 1997;7(8):1067-76. https://doi.org/10.1093/glycob/7.8.1067.
98. Wu A, Pangalos MN, Efthimiopoulos S, Shioi J, Robakis NK. Appican expression induces morphological changes in C6 glioma cells and promotes neural cell adhesion to the extracellular matrix. J Neurosci. 1997;17(13):4987-93. https://doi.org/10.1523/JNEUROSCI.17-13-04987.1997.
99. Gentile F, Onesto V, Accardo A, Vieu C. Small world networks of neuroblastoma cells grown on three-dimensional polymer scaffolds with multiscale roughness. Neural Regen Res. 2020;15(4):759. https://doi.org/10.4103/1673-5374.266923.

Data Availability

The data supporting the results of this study are available in the article itself and/or in the UFMG institutional repository, accessible via the following URL: https://hdl.handle.net/1843/79778